2006

Intercarrier Interference Suppression for the OFDM Systems in Time-Varying Multipath Fading Channels

Xiaozhou Huang
Louisiana State University and Agricultural and Mechanical College

INTERCARRIER INTERFERENCE SUPPRESSION FOR THE OFDM SYSTEMS IN TIME-VARYING MULTIPATH FADING CHANNELS

A Dissertation

Submitted to the Graduate Faculty of the
Louisiana State University and
Agricultural and Mechanical College
in partial fulfillment of the
requirements for the Degree of
Doctor of Philosophy

in

The Department of Electrical and Computer Engineering

by
Xiaozhou Huang
B.S., Northern Jiaotong University, 1993
M.S., Northern Jiaotong University, 1996
M.S., University of Massachusetts Dartmouth, 2002
August 2006

Acknowledgments

I would like to give my sincere thankfulness to my thesis advisor and committee chair, Dr. Hsiao-Chun Wu, for his patient academic guidance through the research and preparation of this dissertation. Because of his invaluable advice and constructive direction, I have been able to finish this dissertation for my Ph.D degree.

I also want to thank Dr. Subhash C. Kak, Dr. Ashok Srivastava, Dr. Peter Wolenski, and Dr. Warren Liao for their willingness to serve as my advisory committee member and their sincere encouragement.

My thanks also goes to my fellow friends I have made during my stay at LSU. Among them are Chi Zhang, Sameer R. Herlekar, Songnan Xi and Xiaolan Wang for their companionship and their assistance. I will always remember the happy time we share together in LSU.

Last but not least, I would like to thank my family, my mother, my brother and my husband for their support and understanding. Without their support, this dissertation would never be finished. I also want to express my love to my husband whose love, caring and support during all these years are the greatest assets in my life.

Table of Contents

List of Tables

List of Figures

List of Acronyms

BER: Bit Error Rate

BS: Base Station

CDMA: Code-division Multiple Access

CIR: Channel Impulse Response

D-AMPS: Digital-Advanced Mobile Phone Service

DF: Decision feedback

DFT: Discrete Fourier Transform

ETSI: European Telecommunication Standards Institute

FDMA: Frequency Division Multiple Access

FDM: Frequency Division Modulation

GSM: Global System for Mobile Communications

IBI: Inter-block interference

ICI: Inter-carrier interference

IDFT: Inverse Discrete Fourier Transform

IFFT: Inverse Fast Fourier Transform

IMT: International Mobile Telecommunications

ISI: Inter-symbol Interference

JDC: Japanese Digital Cellular

MLSE: Maximum Likelihood Sequence Estimator

MMSE: Minimum Mean-square Error

MS: Mobile Station

MSE: Mean-squared Error

OFDM: Orthogonal Frequency Division Multiplexing

PAPR: Peak-to-average-power-ratio

RF: Radio Frequency

SER: Symbol Error Rate

SNR: Signal-to-noise Ratio

TDMA: Time Division Multiple Access

UMTS: Universal Mobile Telecommunications System

WMAN: Wireless Metropolitan Area Networks

WSS: Wide-sense Stationary

WSSUS: Wide-sense Stationary Uncorrelated Scatters

Symbol Notations

$\bar{a}$	vector of a
a_i	the ith element in the vector $\vec{a}$
$\tilde{A}_{N\times M}$	matrix $\tilde{A}$ of size $N \times M$
$A_{i,j}$	the element in the ith row, jth column of the matrix $\tilde{A}$
$[\quad]^T$	transposition of a vector or a matrix
$[\quad]^*$	complex conjugation
$[\quad]^H$	Hermitian transposition of a vector or a matrix
$E\{\}$	expectation operator
$\otimes$	the convolutional operator
$\|\cdot\|^2$	Euclidean vector norm
$tr(\cdot)$	trace operator
$(\cdot)_N$	modulo operation with modulus N
$\Re\{\}$	real part operator
$\Im\{\}$	imaginary part operator
$\angle()$	angle operator

Abstract

Due to its spectral efficiency and robustness over the multipath channels, orthogonal frequency division multiplexing (OFDM) has served as one of the major modulation schemes for the modern communication systems. In the future, the wireless OFDM systems are expected to operate at high carrier-frequencies, high speed and high throughput mobile reception, where the fasting time-varying fading channels are encountered. The channel variation destroys the orthogonality among the subcarriers and leads to the intercarrier interference (ICI). ICI poses a significant limitation to the wireless OFDM systems. The aim of this dissertation is to find an efficient method of providing reliable communication using OFDM in the fast time-varying fading channel scenarios.

First, we investigate the OFDM performance in the situation of time-varying mobile channels in the presence of multiple Doppler frequency shifts. A new mathematical framework of the ICI effect is derived. The simulation results show that ICI induces an irreducible error probability floor, which in proportional to the Doppler frequency shifts. Furthermore, it is observed that ICI power arises from a few adjacent subcarriers. This observation motivates us to design the low-complexity Q-tap equalizers, namely, Minimum Mean Square Error (MMSE) linear equalizer and Decision Feedback (DF) non-linear equalizer to mitigate the ICI. Simulation results show that both Q-tap equalizers can improve the system performance in the sense of symbol error rate (SER).

To employ these equalizers, the channel state information is also required. In this dissertation, we also design a pilot-aided channel estimation scheme via Wiener filtering for a

time-varying Wide-sense Stationary Uncorrelated Scatterers (WSSUS) channel model. The channel estimator utilizes that channel statistical properties. Our proposed low-complexity ICI suppression scheme, which incorporates the Q-tap equalizer with our proposed channel estimator, can significantly improve the performance of the OFDM systems in a fast time-varying fading channels.

At the last part of the dissertation, an alternative ICI mitigation approach, which is based on the ICI self-cancellation coding, is also discussed. The EM-based approach, which solves the phase and amplitude ambiguities associated with this approach, is also introduced.

Chapter 1

Introduction

As perceived in a wide variety of mobile wireless-access applications from voice communications to multimedia data networks in the internet and video broadcasting nowadays, the demand for high-performance broadband multimedia wireless communication systems has drawn popular interests in designing the high-speed, high-quality wireless networks which can achieve the similar quality-of-service of the conventional wired networks. In any mobile radio environment, the multipath effect dominates when the signal waveforms propagate through the air media. If the *channel maximum delay spread* is longer than the transmitted symbol duration, the received signals suffer from the severe inter-symbol interference (ISI). Some existing well-known approaches to combat this ISI problem are related to the employment of the equalizer, code-division multiple access (CDMA) and orthogonal frequency division multiplexing (OFDM) techniques. Generally speaking, the implementation complexity of an equalizer is proportional to the channel delay spread; for example, the corresponding complexity of the *maximum likelihood sequence estimator* (MLSE), which is one of the best equalization schemes for minimizing the bit error rate (BER), increases exponentially with the channel delay spread. In the CDMA systems, the RAKE receiver's structure becomes complicated as the number of RAKE fingers increases when the data rate increases for a fixed delay resolution. The OFDM technique is one of the promising candidates for high-speed communications due to its immunity to the multipath fading channels; by converting a broadband signal into a set of narrowband orthogonal signals for

parallel transmission, each narrowband signal suffers from an approximate frequency-flat fading, and thus needs a one-tap equalizer to compensate the endured multiplicative channel distortion. A general discussion on the existing broadband communication techniques including OFDM will be presented in this chapter. This chapter is organized as follows. Section 1.1 presents an introduction of the contemporary wireless broadband communication techniques. In Section 1.2, a major wireless broadband technique, OFDM, together with its system description, is introduced. At the end of this chapter, we provide the outline of this dissertation work.

1.1 Broadband Communications

This section introduces the general broadband communication system and several technologies such as OFDM, adopted in the existing broadband communication system.

A communication system is called itbroadband if the system bandwidth is larger than that over which the channel transfer function can be considered constant, typically on the order of 100KHz. In the early and mid-1990s, the wireless radio was used almost exclusively to transmit speech signals. The large bandwidth requirement for the broadband system stems from the multiple-access demand, such as frequency division multiple access (FDMA), which increases the transmission bandwidth to accommodate more and more users, rather from the individual user's demand for large bandwidths. However, the individual user's bandwidth requirements are dramatically changing as data transmission and multimedia applications enter the mobile radio market. The third-generation (3G) wireless systems allow faster internet access, video telephone, and many other applications

that require the high-speed data rates in hundreds or thousands of kilobits per second (Kbps) for each user. High-speed wireless computer links even demand 20Mbps (megabits per second). As a result, a modern wireless communication system will provide the same quality-of-service as any wired network like xDSL (Digital Subscriber Line). This stringent data-rate requirement is challenging and would need an evolutionary progress in the wireless broadband communication technologies. Ultimately, the aim of any future mobile communications system is to provide the quality-of-service in parallel with the wired systems.

In typical mobile radio channels, multipath propagation arises from many reflections of the transmitted signal. Due to the multipath propagation from the transmitter to the receiver, the received signal consists of several echoes with different delays and amplitudes. In other words, the impulse response of any mobile radio channel is not a sole Dirac-delta sequence, but a sequence of multiple pulses; thus such a mobile channel is often described as time dispersive. If the maximum delay spread of the channel is much smaller than the transmitted symbol duration, this time dispersion effect on the system performance is insignificant and the system can be deemed operating in a narrowband. On the other hand, the maximum delay spread is longer than the transmitted symbol duration, the system's operation can be deemed in a broadband. Despite the dependence on the transmission channel, it can be always estimated whether a mobile radio system is operating in the broadband or not. In outdoor environments, the maximum delay is typically in the order of $5-20\mu$sec; whereas in indoor environments, it is in the order of $0.1-1\mu$sec or less. Thus,

we can find that an outdoor communication system at a data-rate in excess of 10Kbps, and an indoor system at 200Kbps both can be considered operating in the broadband accordingly.

In the broadband communication system, the time dispersion property of the channel leads to the ISI, which would degrade the overall system performance. Therefore, for the broadband communications, we have to design a mechanism to combat the time-dispersion problem induced by the channel. There are four existing approaches to deal with the ISI for the broadband mobile radio systems, which are listed as follows.

- Unequalized Systems:

  Considerable research [1]-[3] was conducted to quantify the bit error rate (BER) for an unequalized (intrinsic) system in the presence of noise, and the ISI due to the channel time dispersion. The studies on the unequalized systems continued until the middle and late 1990s. The ISI resulting from the time dispersion was treated as the additive noise [1]-[3] and such a system was designed in the narrowband model. This is a very simple approach that would often result in a system performance even worse than a narrowband system.

- Equalizers:

  This approach in [4] exploited the inherent delay diversity associated with the time-dispersive channels, and utilized the equalizers to combat the ISI, and thus improved the system performance over the unequalized system. There were three

equalization schemes including the *MLSE* which was optimal in the sense of minimum error probability, the *linear equalization filter with adjustable coefficients*, and the *decision feedback (DF) equalization* which employed the previously detected symbols to suppress the ISI in the presently detected symbols.

Prior to 1990, speech signal had been transmitted by analog modulation (AM) together with FDMA and the channel frequency spacing was around 25-30KHz. Data transmission was through a channel capacity similar to such a frequency spacing. Since 1990, the voice communications have been digitalized and entered a new era. In the United States, the D-AMPS system integrated a digital speech encoder to transmit speech signals over a 30KHz channel by TDMA; similarly, the JDC standard in Japan allocated the speech signal transmission into a 25KHz channel; the equalization was usually employed in these TDMA/FDMA systems. The adopted equalizers in the D-AMPS standard counter-measured the time dispersion of the channel. The underlying equalizers employed a few taps only since the time dispersion almost never exceeded two symbol intervals; in addition, they were adapted fast since the channel was highly time-variant during one TDMA time slot. However, the JDC standard did not address any equalizer but the necessity still remained.

The GSM specifications were published by ETSI in 1990 [5], which showed the major breakthrough in mobile radio systems. GSM is a TDMA system with a channel spacing of 200KHz. The standard in [5] specified an equalizer capable of coping with the delays up to four symbol durations. The complexity of this equalizer is higher

than that in the D-AMPS systems. The time slot in GSM in sufficiently short such that the channel usually does not change significantly within one time slot. Thus, the adaption algorithm for the equalizer can be greatly simplified in the GSM systems.

- Code Division Multiple Access (CDMA):

  This approach utilized a RAKE receiver to collect the signal energy from the different propagation paths to combat the multipath problem. CDMA has been adopted for UMTS (IMT-2000), which allows the high data-rates up to 2Mbps.

  In the early 1990s, CDMA, previously used for military applications, was modified and extended to the civilian wireless communication applications. The US interim standard IS-95 regulated a typical CDMA communication system for commercial use. In the IS-95 standard, the transmitted information symbols are spread onto a 1.25MHz broadband spectrum by multiplying each bit with a sequences of chips, each chip of 0.814μsec long. In the CDMA systems, the RAKE receiver is used to detect all the distinguishable delay paths and then combines the associated signal components prior to the final detection. This function is similar to an equalizer, but the two implementations are quite different. The CDMA was later adopted by Japanese and European standards to embark their 3G wireless systems, namely code-worded W-CDMA (wideband CDMA). The W-CDMA system has a bandwidth of 5MHz and is also an indoor broadband system, as opposed to the IS-95. For the hardware implementation concern, there has always been interest in the efficient realization of the RAKE receiver especially with a large number of fingers, since such an implementation is the hardcore of the CDMA systems. This implementation problem is of

striking importance especially when the integration with the multiuser detection and spatial signal processing is considered.

- Orthogonal Frequency Division Multiplexing (OFDM):

  There emerges a new modulation/multiple-access technique, namely, OFDM. Essentially, the OFDM allocates the transmitted information symbols onto many subcarriers. The signals on the subcarriers are transmitted in parallel. Since the total system throughput is the cumulative throughput among all subcarriers, the data rate per subcarrier is only a fraction of that of the conventional single-carrier systems such as TDMA with same throughput. Henceforth, the symbol duration on each subcarrier is much longer than the conventional single-carrier schemes, and thus can often reduce the ISI. The OFDM scheme allows us to design a wireless system supporting the high-speed multimedia services.

OFDM exhibits the advantage over the conventional equalization approach for high-rate data communications. The equalization approach can cope with the ISI over a longer symbol sequence, but it is restricted by the induced computational complexity. For example, a system with the transmitted data rate of 10Mbps endures a channel with a maximum delay of 10μsec, the ISI could extend more than 100 symbols and the calculation of the appropriate equalizer coefficients would be very complicated. Nevertheless, CDMA is attractive due to its large spectral efficiency, multiple-access flexibility and outstanding frequency reuse factor of 1. However, the problems of the multi-access interference and the complexity for the multi-user detection have posed the limitation on the CDMA systems.

Moreover, the larger the number of multipath delays, the more complex the hardware implementation of the RAKE receiver. On the other hand, OFDM facilitates a simple equalization for combating the frequency-selective fading channels.

OFDM has been proposed since the 1960s [6] and was suggested for the wireless applications in the 1980s [7]. From then on, the OFDM technique has become one of the prevalent broadband data communication technologies over the multipath fading environments. Because of its immunity to the fading channels and the ISI, OFDM has been widely adopted in several existing wireless-access standards such as digital audio broadcasting (DAB) [8], digital video broadcasting (DVB-T) [9], the IEEE 802.11a [10] local-area network (LAN) standard and the IEEE 802.16a [11] metropolitan-area network (MAN) standard. It allows the data rates up to 75Mbps in the IEEE 802.16e WMAN standard [12]. Since it is capable of higher data-rate communications than TDMA and CDMA systems, OFDM has also been investigated as a potential candidate for the fourth-generation (4G) mobile wireless systems. However, there still remain several challenges to the current OFDM technology, which include the sensitivity to the frequency and time synchronization errors and the often high peak-to-average-power-ratio (PAPR). In this dissertation, we focus on a major OFDM challenge, namely the OFDM performance studies over the fast time-varying multipath fading channels, which are characterized as the most difficult problem in the wireless mobile OFDM applications. More detailed discussions on the OFDM systems will be provided in the following section.

1.2 Orthogonal Frequency Division Multiplexing (OFDM)

This section provides the OFDM introduction in further details. In typical wireless environments, the various propagation paths lead to a time-dispersive channel, which causes the ISI. If the data rate is low and the transmitted symbol duration is large in comparison with the maximum channel delay, the ISI can be neglected. However, as the data rate increases, the ISI becomes more and more severe and additional techniques are required to combat ISI. One of the promising approaches to combat ISI is OFDM. OFDM allocates a high-rate data stream to many low-rate data streams that are transmitted in parallel over many subcarriers. Since the total system throughput is the cumulative throughput among all subcarriers, the data rate per subcarrier is only a fraction of that of the conventional single-carrier system with the same throughput [13]. OFDM has been already adopted in the early military applications since 1960 [6]. However, the efficient and economical OFDM implementation was not available due to the premature semiconductor technology at that time. Today, the OFDM systems with high data rates are technically feasible. In principle, OFDM is similar to FDMA. In a classical FDMA communication system, the transmitted narrowband signals are independently generated, assigned to various frequency bands, transmitted, and separated by the subband filters at the receiver. Similarly, in OFDM, the available channel bandwidth is divided into many narrowband subcarriers. However, the subcarriers are designed to achieve the minimum frequency separation required to maintain the orthogonality among the RF waveforms of the subcarriers while the signal spectra for the different subcarriers still overlap with each other. In 1971, Weinstein and Ebert

proposed a complete OFDM system, in which the OFDM was implemented using FFT and IFFT, and a guard interval was introduced to eliminate the inter-block interference (IBI) [14]. This general system model in [14] is adopted as the underlying OFDM framework in this dissertation.

The OFDM advantages over the conventional single-carrier systems stand out in the frequency selective fading channels. Since each subcarrier in an OFDM system has a very narrow bandwidth, the symbol duration is increased and the ISI caused by the time-dispersive fading channels is greatly mitigated. In addition, a guard interval is inserted at the start of each transmitted OFDM symbol block. If the guard interval is longer than the maximum delay spread of the channel, the IBI is completely eliminated [15]. For the time-invariant frequency-selective multipath channels, which do not change during one OFDM symbol block, a simple one-tap equalizer on each subcarrier can be employed to enhance the symbol detection performance at the OFDM receiver. Previous research has been focused on the OFDM system design over the time-invariant frequency-selective channels [16][17]. However, it is well known that the OFDM system is very sensitive to the local oscillator carrier-frequency offset, the local oscillator phase noise, the time synchronization error, and the Doppler frequency spread since they can destroy the subcarrier orthogonality [13] [15]. Hence, these aforementioned factors still remain as the major challenges in the OFDM technology.

In the future, the OFDM systems are expected to operate at high carrier-frequencies, high-speed mobile reception and high throughput and it would result in both time- and

frequency-selective (time-varying) channels, wherein the time-invariant channel assumption no longer holds. In such conditions, the channel variation during one OFDM symbol destroys the orthogonality among subcarriers, and leads to the intercarrier interference (ICI) and the OFDM performance degradation [18]. In the presence of ICI, the simple one-tap equalizer does not provide the satisfactory performance anymore. In this dissertation, we investigate the OFDM system behaviors in the time-varying channels where the ICI occurs. In OFDM, the symbol-to-symbol variations of the channel characteristics are more severe than those in the single-carrier systems due to its longer symbol duration. Time variations of the channels during one OFDM symbol duration destroys the orthogonality among subcarriers, cause the ICI and result in an irreducible error probability floor in the conventional OFDM systems with one-tap equalizers. This dissertation is focused on the investigation of an efficient method of enhancing the OFDM systems in the fast time-varying fading scenarios. Here, we restrict the future discussions on the time-varying multipath fading channels together with the multiple Doppler frequency shifts.

1.3 Organization of the Dissertation

The outline of this dissertation is stated as follows. In Chapter 2, we formulate the OFDM system transmission model over the fast time-varying fading channels in the presence of multiple Doppler frequency shifts. A new mathematical framework characterizing the ICI effects is derived thereupon; the OFDM system performance is also analyzed and evaluated over such time-varying fading channels. In Chapter 3, the existing ICI mitigation algorithms for combating the time-varying channels are discussed and summarized.

We propose a novel ICI mitigation algorithm, which will show some advantages over the existing methods in a certain channel conditions in Chapter 4; in our proposed algorithm, we design a Q-tap MMSE linear equalizer and a Q-tap DF non-linear equalizer to mitigate the ICI. In Chapter 4, we also study a pilot-aided Wiener filter based MMSE channel parameter estimation algorithm for the OFDM systems in the fast time-varying fading channels. Our proposed pilot-aided Wiener filtering based channel parameter estimators make use of the channel statistical properties. An alternative ICI mitigation approach, which is based on the ICI self-cancellation [19][20], is presented in Chapter 5. Finally, a brief summary and the remarks on the future research is drawn in Chapter 6. The symbol notations used throughout this dissertation are listed in the "Symbol Notations" in pp. X.

Chapter 2

OFDM in Fast Time-varying Fading Channels

OFDM is a promising modulation scheme over frequency-selective channels. In the OFDM systems, the available channel bandwidth is divided into many narrowband subcarriers, which are transmitted in parallel. OFDM modulator splits a high-rate data stream into many low-rate parallel substreams, and each substream is modulated onto the orthogonal subcarriers using the inverse fast Fourier transform (IFFT). If the bandwidth of each subcarrier is much less than the channel coherence bandwidth, the signal on each subcarrier is assumed to experience a flat-fading. Moreover, the inter-block interference (IBI) can be removed using the insertion of a guard interval under the assumption that the length of the guard interval is larger than the channel maximum delay spread. Therefore, the multipath channel effect on each subcarrier can be represented as a single complex multiplicative distortion. A simple one-tap equalizer can be employed to enhance the symbol detection performance at the OFDM receivers. Despite these advantages, the OFDM increases the symbol duration and causes the adverse effects in the fast time-varying fading channels. For instance, the time variations of the channel characteristics within one OFDM symbol block destroy the subcarrier orthogonality and result in the inter-carrier interference (ICI). This ICI would induce an irreducible error probability floor in the conventional OFDM receivers integrated with one-tap equalizers. The performance degradation due to the ICI becomes significant as the carrier frequency, the OFDM symbol block duration, and the receiver's mobility increase.

The OFDM system performance caused by the ICI in the time-varying channels has been studied in the literature [18][21]-[25]. All of the existing ICI analyses are based on the assumption that the Doppler frequency shifts for all propagation paths are identical and the ICI results only from a time-varying channel. However, in any wireless communication systems, as the mobile subscriber moves across the area covered by several base stations, the differences in the base station locations, the signal propagation paths and the signal incident angles with respect to the direction of the subscriber movement result in the distinct Doppler frequency shifts among the propagation paths. In this chapter, first the OFDM system model and the adopted channel model are described. Then we investigate the OFDM system performance in the fast time-varying fading channels in the presence of multiple Doppler frequency shifts. The OFDM system model is formulated in Section 2.1. Section 2.2 presents the channel model adopted in this dissertation. In Section 2.3, we derive a new mathematical framework for the ICI analysis; the OFDM system performance is also quantified and evaluated over the fast time-varying fading channels in the presence of multiple Doppler frequency shifts accordingly. The concluding remarks for this chapter are given in Section 2.4.

2.1 OFDM System Model

In an OFDM system, the usable bandwidth is divided into N spectrally equispaced subcarriers. Thus, N transmitted signals are modulated onto each subcarrier independently. An OFDM signal consists of N subcarriers with a frequency spacing Δf. The signal waveforms on the subcarriers are orthogonal to each other within a period of $T_f = 1/\Delta f$.

Since the bandwidth is divided into N narrowband subcarriers, the OFDM symbol block duration T_f is N times longer than that of the single-carrier systems allocated with the same bandwidth. Typically, for a communication system, the number of subcarriers N is chosen such that the OFDM symbol block duration T_f is longer than the channel maximum delay spread. To avoid the IBI, the OFDM symbol block is extended by a cyclic prefix, which is also called guard interval with the length T_g. Hence, the complete OFDM block duration is $T = T_f + T_g$. One of major OFDM advantages is IBI-free. If the guard interval length T_g is larger than the maximum channel delay spread, the interference from the previous OFDM symbol block appears within the guard interval only. At the receiver, the signal samples in the guard interval are discarded. Therefore, the IBI is completely eliminated, and the orthogonality of subcarriers can be retrieved at the receiver. In this section, we provide an analytical description of the general OFDM transmission scheme. We also describe how the OFDM signal is generated at the transmitter, as well as how the symbol detection is achieved at the receiver.

In an OFDM system, the transmitted symbols are modulated onto each subcarrier independently. Let $X_{i,k}$ denote the complex-valued transmitted information data, for the kth subcarrier in the ith OFDM symbol block. Since the samples in the guard interval are discarded at the receiver, we need to consider the signals transmitted in the period of T_f only. Thus, within the ith OFDM symbol duration T_f, the signal transmitted on the kth

subcarrier can be formulated as

$$x_{i,k}(t) = \begin{cases} X_{i,k} e^{j2\pi f_k t}, & (i-1)T + T_g \le t \le iT \\ 0, & \text{otherwise,} \end{cases} \tag{2.1}$$

where $f_k = k\Delta f = \frac{k}{T_f}$ is the center frequency for the kth subcarrier. Therefore, the complete OFDM signal is represented as

$$x_i(t) = \sum_{k=0}^{N-1} X_{i,k} g_k(t), \quad (i-1)T + T_g \le t \le iT, \tag{2.2}$$

where $g_k(t) \equiv \frac{1}{\sqrt{T_f}} e^{j2\pi f_k t}$, the $\frac{1}{\sqrt{T_f}}$ is the normalization factor. According to Eq. (2.1), the RF waveform of each subcarrier is mutually orthogonal, i.e.,

$$< g_k(t), g_l(t) > \equiv \int_0^{T_f} g_k(t) g_l^*(t)\, dt = \delta(k-l), \tag{2.3}$$

where $\delta(\cdot)$ denotes the Dirac's delta function. Therefore, the transmitted signal $X_{i,k}$ can be recovered by a correlation operation at the receiver, i.e.

$$X_{i,k} = < x_i(t), g_k(t) >, \quad (i-1)T + T_g \le t \le iT. \tag{2.4}$$

Eq. (2.1)-Eq. (2.4) describe the basic OFDM modulation operations. Usually, the OFDM modulation is implemented in the discrete time domain rather than in the continuous time domain [14]. The OFDM transmitter and receiver implementations in the discrete time domain [14] will be presented next.

A. **OFDM Transmitter**

Since there are N subcarriers in one OFDM symbol block, each with bandwidth Δf, the OFDM signal bandwidth is $B = N\Delta f$, and the corresponding sampling

period is $T_s = 1/B = \frac{1}{N\Delta f}$. Thus, the discrete-time transmitted signal $x_{i,n}$ for the nth time sample in the ith OFDM symbol block is represented as

$$\begin{aligned} x_{i,n} &\equiv x_i(nT_s) \quad n = 0, 1, \cdots N-1 \\ &= \frac{1}{\sqrt{T_f}} \sum_{k=0}^{N-1} X_{i,k} e^{j2\pi k \Delta f n T_s} \\ &= \frac{1}{\sqrt{NT_s}} \sum_{k=0}^{N-1} X_{i,k} e^{\frac{j2\pi kn}{N}}, \end{aligned} \tag{2.5}$$

where the factor $\frac{1}{\sqrt{NT_s}}$ is the normalization factor. Eq. (2.5) illustrates the inverse discrete Fourier transform (IDFT) operation. In practice, the OFDM signal $x_{i,n}$ is generated using IFFT as shown in Fig. 2.1. Figure 2.1 depicts a basic OFDM system diagram including both transmitter and receiver.

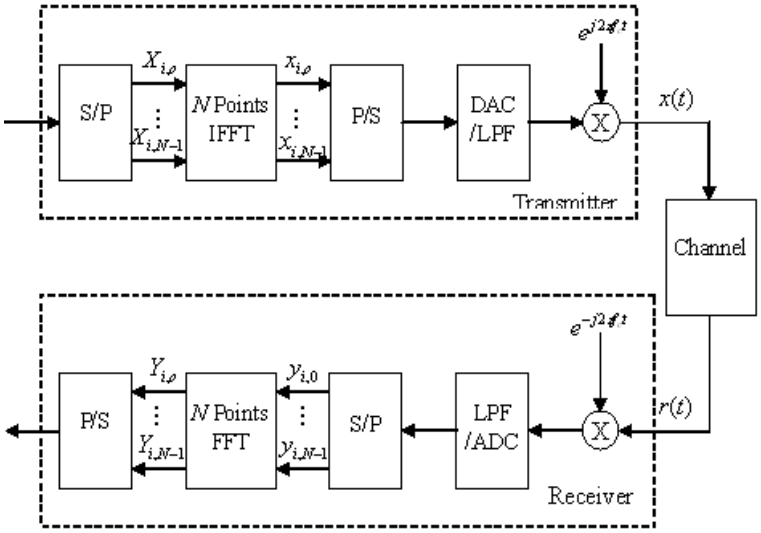

Figure 2.1: Baseband OFDM transmission model with N subcarriers

According to Figure 2.1, a block of N complex-valued transmitted symbols $X_{i,k}$ are fed into the OFDM modulator; an N-point IFFT is employed to generate N

subcarrier sequences. The nth discrete-time transmitted signal in the ith OFDM symbol block is therefore given by

$$x_{i,k} = \frac{1}{\sqrt{N}} \sum_{k=0}^{N-1} X_{i,k} e^{\frac{j2\pi nk}{N}}, \tag{2.6}$$

where $\frac{1}{\sqrt{N}}$ is also a normalization factor. To avoid the IBI, the guard interval consists of a cyclic extension of the OFDM-modulated sequence, i.e., the last G samples of the IFFT outputs, are appended at the beginning of every OFDM symbol block. The guard interval duration is $T_g = GT_s$. In this dissertation, it is always assumed that the guard interval duration T_g is longer than the maximum channel delay spread. Therefore, the IBI is completely eliminated. After the guard interval is appended, the transmitted OFDM signals $x_{i,n}$ are sent through a parallel-to-serial port (P/S) and a digital-to-analog converter (DAC), and then passed through a low-pass pulse shaping filter. The resulting waveforms are then transmitted over a multipath fading channel.

B. **OFDM Receiver**

At the receiver, the received signal $r(t)$ can be separated into the N orthogonal subcarrier signals by a correlation technique according to Eq. (2.3):

$$Y_{i,m} = < r(t), g_m(t) >, \quad (i-1)T + T_g \leq t \leq iT. \tag{2.7}$$

Alternatively, the correlation operator at the OFDM receiver can be implemented using a discrete Fourier transform (DFT) as shown in Figure 2.1. After being through the low-pass pulse shaping filter, the received signal is sampled at the rate T_s, i.e., $y_{i,k} = r((i-1)T + kT_s)$. Then, the samples in the cyclic prefix interval are discarded,

and the resulting sequence will go through an N-point DFT. Ultimately, the OFDM demodulated symbol $Y_{i,m}$, which is on the mth subcarrier in the ith OFDM symbol block, can be obtained as

$$Y_{i,m} = \frac{1}{\sqrt{N}} \sum_{n=0}^{N-1} y_{i,n} e^{\frac{-j2\pi nm}{N}}. \tag{2.8}$$

If a time-invariant channel is considered, i.e., the channel does not change during one OFDM symbol block duration T, the multipath channel effect only appears as a multiplication of each subcarrier signal by a complex-valued channel factor. As a result, the transmitted signal can be recovered by employing an one-tap equalizer at the receiver to compensate the channel distortion. However, the subcarrier orthogonality still remains even with this channel effect and this is the pivotal advantage of the OFDM technology. For the single-carrier systems with the same bandwidth, a channel with a large maximum delay spread would result in severe ISI, while the ISI is negligible in OFDM since the bandwidth of each subcarrier is narrow enough to experience a flat fading, as long as the maximum channel delay spread is less than the guard interval. This advantage holds under the strict assumption of perfect time and frequency synchronizations at the receiver. However, in the future, the OFDM systems are expected to operate at high-speed mobile reception and it would result in both time- and frequency-selective (time-varying) channels, wherein the time-invariant channel assumption no longer holds. In such conditions, the channel variation during one OFDM symbol block destroys the orthogonality among subcarriers, and leads to the ICI. In the presence of ICI, the simple one-tap equalizer, which

compensates the channel distortion as in conventional OFDM receivers, does not provide the satisfactory performance anymore. In the next section, we will introduce the channel model adopted throughout the dissertation; we focus on the time-varying multipath fading channels together with the multiple Doppler frequency shifts, and the perfect time and carrier frequency synchronizations are assumed.

2.2 Channel Model

The OFDM system performance is determined by the channel over which the signals are transmitted. The adopted channel model needs to be carefully studied prior to any further discussion. We discuss the underlying channel model in this section.

In mobile wireless communications, there exist multiple propagation paths between

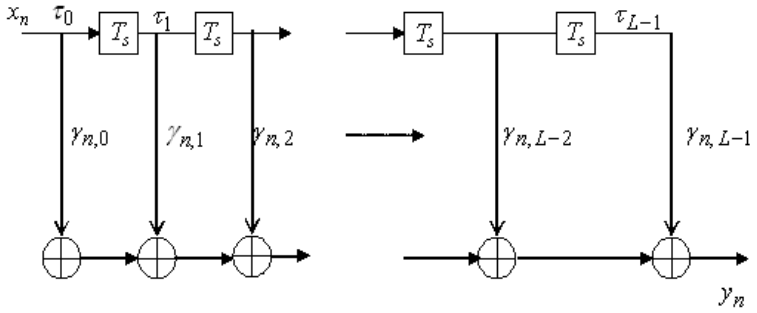

Figure 2.2: Tapped delay line channel model

transmitter and receiver in reality. The general mobile radio channel is characterized as the tapped-delay line model, as shown in Figure 2.2. This channel consists of L delays and each delay path is characterized by its delay spread τ_l, together with the associated channel attenuation factor $\gamma_l(t)$. For the selection of τ_l, there are essentially two possibilities; first, they coincide with the arrival times of the physical paths; second, they are spaced

equidistantly, i.e., $\tau_l = lT_s$, where T_s is the sampling period. We will adopt the latter case (equidistantly spaced) in the dissertation. Consequently, the channel impulse response (CIR) can be written as

$$h(t,\tau) = \sum_{l=0}^{L-1} \gamma_l(t)\,\delta(t-\tau_l), \tag{2.9}$$

where L is the number of delay paths, $\gamma_l(t)$ is the time-varying attenuation coefficient for the lth delay path, and τ_l is the delay spread between the transmitted and received signals. The corresponding discrete channel model is given as

$$h(n,\tau) = \sum_{l=0}^{L-1} \gamma_{l,n}\delta(n-\tau_l), \tag{2.10}$$

where $h(n,\tau) \equiv h(nT_s,\tau)$, and $\gamma_{l,n} \equiv \gamma_l(nT_s)$ and the sampling period is T_s. It is usually assumed that $\tau_0 = 0$. Moreover, the channel attenuation coefficient $\gamma_l(t)$ is assumed to constitute a zero-mean stochastic process. The overall power is always normalized to 1, i.e.,

$$E\{\gamma_l(t)\} = 0, \tag{2.11a}$$

$$\sum_{l=0}^{L-1} \sigma_{h,l}^2 = 1, \tag{2.11b}$$

where $E\{\cdot\}$ is the expectation operator, and $\sigma_{h,l}^2$ is the power of the channel attenuation factor $\gamma_l(t)$ for the lth delay path, i.e., $\sigma_{h,l}^2 \equiv E\{|\gamma_l(t)|^2\}$.

Usually, we would use the correlation function of the channel attenuation factor to describe the channel properties. The correlation of the channel attenuation factor is given by

$$r_h(t_1,t_2,\tau_l,\tau_{l'}) \equiv E\{\gamma_l(t_1)\,\gamma_{l'}^*(t_2)\}. \tag{2.12}$$

However, this correlation function is usually too complicated in practice because it depends on the four variables $t_1, t_2, \tau_l, \tau_{l'}$. A further simplification is achieved using the wide-sense stationary uncorrelated scatters (WSSUS) assumption [26]. Based on the WSSUS assumption, the channel correlation function in Eq.(2.12) is simplified as [4][26]

$$r_h(t_1, t_2, \tau_l, \tau_{l'}) = \phi_h(\Delta t, \tau_l)\,\delta(\tau_l - \tau_{l'}), \tag{2.13}$$

where $\Delta t = t_1 - t_2$. Eq. (2.13) implies that the channel attenuation factors associated with different delay paths are uncorrelated with each other. For $\Delta t = 0$, we define the function $\phi_\tau(\tau_l)$ as $\phi_h(0, \tau)$, i.e., $\phi_\tau(\tau_l) \equiv \phi_h(0, \tau_l)$. The function $\phi_\tau(\tau_l)$, $0 \le l \le L-1$, is known as the *multipath intensity profile* of the channel. More explicitly, $\phi_\tau(\tau_l)$ is the average power of the channel attenuation coefficient for a given lth delay path, which is defined in Eq. (2.11b). Therefore, Eq. (2.11b) could be also written as

$$\sum_{l=0}^{L-1} \phi_\tau(\tau_l) = 1. \tag{2.14}$$

In a rich scattering environment, the arrival angle of the received signal waveform is a uniformly distributed random variable, which implies that the channel's autocorrelation function is separable in time and delay [27][28], i.e.,

$$\phi_h(\Delta t, \tau_l) = \phi_t(\Delta t)\,\phi_\tau(\tau_l), \tag{2.15}$$

where $\phi_\tau(\tau_l)$ is the aforementioned multipath intensity profile and $\phi_t(\Delta t)$ is called *space-time correlation function*. For the WSSUS channel model, each delay path is assumed to have the same space-time correlation function. The Fourier transform of the space-time

correlation function $\phi_t(\Delta t)$ is the *Doppler power spectrum*, which is denoted as $\Phi(f)$, i.e.,

$$\Phi(f) = \int_{-\infty}^{\infty} \phi_t(\Delta t)\, e^{-j2\pi\Delta t f} d\Delta t. \tag{2.16}$$

Since the classical Jake's model in [28] is for the situation in which the receiver (or the transmitter) is mobile and this is the case we are interested in, we will adopt the Jake's model for our future discussions. For the Jake's model, the space-time correlation function is given as

$$\phi_t(\Delta t) = J_0(2\pi f'_D \Delta t), \tag{2.17}$$

where $J_0()$ is the zeroth-order Bessel function of the first kind, and f'_D is the maximum Doppler frequency shift.

As we mention in Section 1.2, we restrict our discussions on the time-varying channels. The time-varying behavior of each delay tap attenuation $\gamma_l(t)$ is affected by the Doppler power spectrum. In mobile communication systems, as the mobile subscriber moves across the area covered by several base stations, the differences in the base station locations, the signal propagation paths and the signal incident angles with respect to the direction of the subscriber movement result in the distinct Doppler frequency shifts among propagation paths. Every incident waveform on the mobile subscriber undergoes a Doppler frequency shift due to the motion. The Doppler frequency shift for the lth path in Hertz is given by

$$f'_l = \frac{v}{\lambda}\cos\theta_l = f'_D \cos\theta_l, \tag{2.18}$$

where λ is the incident wavelength, v is the mobile station's moving speed, θ_l is the incident angle for the lth incident wave, and f'_D is the maximum Doppler frequency shift which is

defined as $f'_D = \frac{v}{\lambda}$. It is assumed that the incident angles θ_l constitute a random variable uniformly distributed in the interval between $-\pi$ and π. Therefore, the probability density function of θ_l is given as

$$p_{\theta_l}(\theta_l) = \begin{cases} \frac{1}{2\pi}, & \theta_l \in [-\pi, \pi], \\ 0, & otherwise. \end{cases} \tag{2.19}$$

Consequently, the Doppler frequency shifts, defined in Eq. (2.18), also constitute another random variable. The probability density function of the Doppler frequency shift, denoted as $p_{f'_l}(f'_l)$, can be formed thereby. After some elementary calculations, we achieve the following result for the probability density function $p_{f'_l}(f'_l)$ of the Doppler frequency shift:

$$p_{f'_l}(f'_l) = \begin{cases} \frac{1}{\pi f'_D \sqrt{1-\left(f'_l/f'_D\right)^2}}, & |f'_l| \le f'_D \\ 0, & otherwise. \end{cases} \tag{2.20}$$

In this dissertation, it is assumed that the Doppler frequency shift for each delay path has the identical probability density function, as given by Eq. (2.20).

At the OFDM receiver, in the absence of time synchronization errors, the ith received OFDM symbol block $r_i(t)$ can be formulated as

$$\begin{aligned} r_i(t) &= \int_0^{T_f} h(t,\tau)\, x_i(t-\tau) d\tau + w(t) \\ &= \sum_{l=0}^{L-1} \gamma_l(t)\, x_i(t-\tau_l)\, e^{j2\pi f'_l (t-\tau_l)} + w(t), \end{aligned} \tag{2.21}$$

where f'_l is the Doppler frequency shift for the lth delay path defined in Eq. (2.18) and $w(t)$ is the additive white Gaussian noise (AWGN). Then, we apply the assumption $\tau_l = lT_s$ to derive the corresponding discrete-time received signal. The sampling rate is T_s. The nth

discrete-time received signal $y_{i,n}$ in the ith OFDM symbol block is given by

$$y_{i,n} = \sum_{l=0}^{L-1} \gamma_{l,n} x_{i,n-l} e^{j2\pi f'_l (n-l)} + w_n, \tag{2.22}$$

where $y_{i,n} \equiv r(nT_s)$, $\gamma_{l,n} \equiv \gamma_l(nT_s)$ and $w_n \equiv w(nT_s)$. It is noted that the received signal in the current OFDM symbol block is not interfered by the symbols in the previous OFDM symbol blocks with the aid of cyclic prefix. From now on, the OFDM symbol block index i will be dropped for notational convenience.

According to the transmission model in Eq. (2.22), we will further investigate the ICI effect on the OFDM system performance due to the channel variations in the presence of multiple Doppler frequency shifts in the next section.

2.3 Properties of Intercarrier Interference (ICI)

Before we derive the mathematical framework for the ICI based on the aforementioned transmission model, we give a brief introduction about the ICI effect due to the time-varying channels in the existing literature.

In [18], according to the central-limit theorem, the ICI was modeled as a Gaussian random process and the OFDM system performance degradation due to the ICI has been discussed. Several Doppler spectra were also analyzed and compared in [21]. In [22], the tight and universal bounds for the ICI resulting from the Doppler spread have been derived. In order to achieve a signal-to-interference ratio (SIR) larger than 20 dB, the OFDM symbol duration must be smaller than 8% of the channel coherence time based on the WSSUS channel model in [23], and in [24] it is concluded that if *the OFDM symbol normalized maximum Doppler frequency shift* $f'_D T_f$ is less than 0.01, a time-invariant channel can be

assumed during one OFDM symbol interval. When an OFDM symbol duration is less than 10% of the channel coherence time, the channel variation can be assumed in a linear fashion [25]. However, all of the ICI analyses are based on the assumption that the Doppler frequency shifts for all paths are identical and the ICI is induced only by a time-varying channel. Consequently, this common Doppler frequency shift can be viewed as a portion of local oscillator frequency shift, which is assumed to be time-invariant. A technique was proposed to resolve the local oscillator frequency shift problem in [29], where an additional frequency detector was incorporated with the phase-locked loop (PLL) employed for the coherent OFDM signal detection. However, when the multiple Doppler frequency shifts arise, the orthogonality among subcarriers can not be recovered by simply adjusting the receiver's PLL to compensate a constant Doppler frequency shift. The compensation of a single Doppler shift for a particular path would still result in the frequency offset problems for other different paths. In [30], the ICI problem for the two-path channels with different Doppler frequencies was studied. In this section, we will analyze the ICI properties in detail for a more realistic situation where there are more than two paths with different Doppler frequency shifts. First, we will derive an OFDM transmission model for fast time-varying channels. Second, the ICI properties are invertigated, and the ICI effects on the OFDM performance are presented via computer simulations.

2.3.1 OFDM Transmission Under Time-varying Channels

By substituting Eq. (2.6) into Eq. (2.22), the discrete-time received signal y_n is

$$y_n = \sum_{l=0}^{L-1} \gamma_{l,n} x_{n-l} e^{j2\pi f_l' T_s (n-l)} + w_n \tag{2.23}$$

$$
\begin{aligned}
&= \frac{1}{\sqrt{N}} \sum_{l=0}^{L-1} \gamma_{l,n} e^{j2\pi f_l' T_s (n-l)} \sum_{k=0}^{N-1} X_k e^{\frac{j2\pi k(n-l)}{N}} + w_n \\
&= \frac{1}{\sqrt{N}} \sum_{k=0}^{N-1} X_k e^{\frac{j2\pi nk}{N}} \sum_{l=0}^{L-1} \gamma_{l,n} e^{\frac{-j2\pi kl}{N}} e^{j2\pi f_l' T_s (n-l)} + w_n.
\end{aligned}
$$

After discarding the prefix samples in the guard interval, the rest of the samples pass through the OFDM demodulator. Hence the subject sequence is in the period of OFDM duration T_f. The OFDM demodulated signal could be obtained using a DFT operation according to Eq.(2.8). Thus, the OFDM demodulated signal at the mth subcarrier, Y_m, is given by

$$
\begin{aligned}
Y_m &= \frac{1}{\sqrt{N}} \sum_{n=0}^{N-1} y_n e^{-j2\pi nm/N} \\
&= \frac{1}{N} \sum_{n=0}^{N-1} \left\{ \sum_{k=0}^{N-1} X_k e^{\frac{j2\pi nk}{N}} \sum_{l=0}^{L-1} \gamma_{l,n} e^{\frac{-j2\pi kl}{N}} e^{j2\pi f_l' T_s (n-l)} \right\} e^{\frac{-j2\pi nm}{N}} + W_n,
\end{aligned}
\tag{2.24}
$$

where $W_m = \frac{1}{\sqrt{N}} \sum_{n=0}^{N-1} w_n e^{\frac{-j2\pi mn}{N}}$ is a complex-valued Gaussian noise process added on the mth subcarrier. Since $w(t)$ is a zero-mean white Gaussian noise process with variance σ_w^2, obviously W_m is an independent zero-mean white Gaussian noise process with the same variance $w(t)$, i.e.,

$$
E\{W_m\} = 0, \quad \forall 0 \le m \le N-1, \tag{2.25a}
$$

$$
\sigma_W^2 \equiv E\{W_m, W_m^*\} = \sigma_w^2, \tag{2.25b}
$$

$$
E\left\{W_{m_1}, W_{m_2}^*\right\} = \sigma_W^2 \delta(m_1 - m_2). \tag{2.25c}
$$

Two symbols are denoted here. $\epsilon_l \equiv f_l' T_f$ is defined as the *OFDM symbol normalized Doppler frequency shift*, while $\epsilon_D \equiv f_D' T_f$ is defined as the *maximum OFDM symbol*

normalized Doppler frequency shift. Then Eq. (2.24) yields

$$
\begin{aligned}
Y_m &= \frac{1}{N}\sum_{n=0}^{N-1}\left\{\sum_{k=0}^{N-1}X_k e^{\frac{j2\pi nk}{N}}\sum_{l=0}^{L-1}\gamma_{l,n}e^{\frac{-j2\pi kl}{N}}e^{\frac{j2\pi f_l' T_f(n-l)}{N}}\right\}e^{\frac{-j2\pi nm}{N}}+W_n \qquad (2.26)\\
&= \frac{1}{N}\sum_{n=0}^{N-1}\left\{\sum_{k=0}^{N-1}X_k e^{\frac{j2\pi nk}{N}}\sum_{l=0}^{L-1}\gamma_{l,n}e^{\frac{-j2\pi kl}{N}}e^{\frac{j2\pi \epsilon_l(n-l)}{N}}\right\}e^{\frac{-j2\pi nm}{N}}+W_n\\
&= \frac{1}{N}\sum_{k=0}^{N-1}X_k\sum_{l=0}^{L-1}e^{\frac{-j2\pi(k+\epsilon_l)l}{N}}\sum_{n=0}^{N-1}\gamma_{l,n}e^{\frac{-j2\pi(m-k-\epsilon_l)n}{N}}+W_m\\
&= \sum_{k=0}^{N-1}X_k\sum_{l=0}^{L-1}e^{\frac{-j2\pi(k+\epsilon_l)l}{N}}H_l^{(m-k)}+W_m\\
&= X_m\sum_{l=0}^{L-1}H_l^0 e^{\frac{-j2\pi(m+\epsilon_l)l}{N}}+\sum_{\substack{k=0\\k\neq m}}^{N-1}X_k\sum_{l=0}^{L-1}e^{\frac{-j2\pi(k+\epsilon_l)l}{N}}H_l^{(m-k)}+W_m\\
&= \alpha_m X_m+\sum_{\substack{k=0\\k\neq m}}^{N-1}X_k C_{m,k}+W_m\\
&= \alpha_m X_m+I_m+W_m,
\end{aligned}
$$

where $\alpha_m \equiv \sum_{l=0}^{L-1}H_l^0 e^{\frac{-j2\pi(m+\epsilon_l)l}{N}}$ represents the multiplicative channel distortion at the subject subcarrier m, $I_m = \sum_{\substack{k=0\\k\neq m}}^{N-1}X_k C_{m,k}$ represents the ICI, $C_{m,k} = \sum_{l=0}^{L-1}e^{\frac{-j2\pi(k+\epsilon_l)l}{N}}H_l^{(m-k)}$ is the ICI coefficient specifying the interference from subcarrier k to subcarrier m. Besides, $H_l^{(m-k)}$ denotes the discrete Fourier transform of the time-varying multipath channel, which is given by

$$H_l^{(m-k)} = \frac{1}{N}\sum_{n=0}^{N-1}\gamma_{l,n}e^{\frac{-j2\pi(m-k-\epsilon_l)n}{N}}. \qquad (2.27)$$

Furthermore, we can rewrite Eq. (2.26) in a matrix form such that

$$\vec{Y} = \tilde{C}\vec{x}+\vec{W}, \qquad (2.28)$$

where $\vec{Y} \equiv [Y_0 \quad Y_1 ... Y_{N-1}]^T$, $\vec{X} \equiv [X_0 \quad X_1 ... X_{N-1}]^T$, $\vec{W} \equiv [W_0 \quad W_1 ... W_{N-1}]^T$ and the matrix $\tilde{C}$ is called the *ICI coefficient matrix* with size $N \times N$, which is given by

$$\tilde{C} \equiv \begin{bmatrix} C_{0,0} & C_{0,1} & \cdots & C_{0,N-1} \\ C_{1,0} & C_{1,1} & \cdots & C_{1,N-1} \\ \vdots & \vdots & \ddots & \vdots \\ C_{N-1,0} & C_{N-1,1} & \cdots & C_{N-1,N-1} \end{bmatrix}_{N \times N} . \tag{2.29}$$

Here, the off-diagonal entry in the mth row, the kth column, $C_{m,k}, 0 \leq m, k \leq N-1$ and the diagonal elements $\alpha_m \equiv C_{m,m}, 0 \leq m \leq N-1$ are defined in Eq. (2.26). The off-diagonal elements in $\tilde{C}$ defined in Eq. (2.29) represent the ICI caused by the time-varying nature of the channel in the presence of multiple Doppler frequency shifts. In the time-invariant channel without multiple Doppler frequency shifts, we have $\gamma_l(t) = \gamma_l$ and $f_l' = 0, \forall 0 \leq l \leq L-1$, where γ_l is a zero-mean random variable with the variance $\sigma_{h,l}^2$. This leads to $I_m = 0$ and $C_{m,k} = 0, m \neq k$; thus, the ICI coefficient matrix $\tilde{C}$ is diagonal, i.e.,

$$\begin{aligned} C_{m,k} &= \sum_{l=0}^{L-1} \gamma_l e^{\frac{-j2\pi lm}{N}} \delta(m-k) \qquad (2.30) \\ &= \begin{cases} \alpha_m, & m = k \\ 0, & m \neq k \end{cases} . \end{aligned}$$

Therefore, a one-tap equalizer can be employed at the receiver for the coherent detection to compensate such a multiplicative channel distortion α_m. On the other hand, in the time-varying channel with multiple Doppler frequency shifts, the ICI coefficient matrix is usually not diagonal and the ICI effect can not be ignored. We will investigate the ICI

properties, including the corresponding second-order statistics, in the next sub-section.

2.3.2 ICI Properties

In this sub-section, we study the statistical property regarding the ICI I_m in Eq. (2.26), namely the variance of the ICI. For a sufficiently large N, the central limit theorem can be invoked and the ICI I_m can be modeled as a Gaussian random process. For the symbol detection, the ICI can be simply considered as the additive Gaussian noise. Next, we will derive an explicit mathematical expression for this ICI variance. The ICI variance σ_{ICI}^2 can be formulated as

$$\begin{aligned} \sigma_{ICI}^2 &\equiv E\left\{I_m I_m^*\right\} \\ &= E\left\{\left(\sum_{\substack{k=0\\k\neq m}}^{N-1} X_k C_{m,k}\right)\left(\sum_{\substack{k=0\\k\neq m}}^{N-1} X_k C_{m,k}\right)^*\right\}. \end{aligned} \tag{2.31}$$

The transmitted symbols X_k are assumed to have zero mean and are uncorrelated for different subcarriers and then the ICI variance can be written as

$$\sigma_{ICI}^2 = E_s \sum_{\substack{k=0\\k\neq m}}^{N-1} E\left\{C_{m,k} C_{m,k}^*\right\}. \tag{2.32}$$

Substituting Eq. (2.26) into Eq. (2.32), we obtain

$$\begin{aligned} & E\left\{C_{m,k} C_{m,k}^*\right\} \\ = \; & \frac{1}{N^2} \sum_{l=0}^{L-1} \sum_{l'=0}^{L-1} E\left\{ e^{\frac{-j\pi(k+\epsilon_l)l}{N}} e^{\frac{j2\pi(k+\epsilon_{l'})l'}{N}} \sum_{n_1=0}^{N-1} \sum_{n_2=0}^{N-1} \gamma_{l,n}\gamma_{l',n_2} e^{\frac{-j2\pi(m-k-\epsilon_l)n}{N}} e^{\frac{j2\pi(m-k-\epsilon_{l'})n_2}{N}} \right\} \\ = \; & \frac{1}{N^2} \sum_{l=0}^{L-1} \sum_{n_1=0}^{N-1} \sum_{n_2=0}^{N-1} \phi_t\left(n_1-n_2\right) \phi_\tau\left(l\right) e^{\frac{-j2\pi(m-k-\epsilon_l)n_1}{N}} e^{\frac{j2\pi(m-k-\epsilon_l)n_2}{N}} \\ = \; & \frac{1}{N^2} \sum_{n_1=0}^{N-1} \sum_{n_2=0}^{N-1} \phi_t\left(n_1-n_2\right) e^{\frac{-j2\pi(m-k)(n_1-n_2)}{N}} E\left\{ e^{\frac{j2\pi(n_1-n_2)\epsilon_l}{N}} \right\}, \end{aligned} \tag{2.33}$$

where $\phi_t(n_1 - n_2)$ is the space-time correlation function, which is given in Eq. (2.15) by setting $\Delta t = (n_1 - n_2)T_s$. For notational simplicity, the sampling period T_s is discarded. Given the probability density function of the Doppler frequency shift f_l' in Eq. (2.20), we obtain

$$\begin{aligned} & E\left\{e^{\frac{j2\pi\epsilon_l(n_1-n_2)}{N}}\right\} \\ = & \int_{-f_D'}^{f_D'} \frac{1}{\pi f_D' \sqrt{1-\left(f_l'/f_D'\right)^2}} e^{\frac{j2\pi(n_1-n_2)f_l'T_f}{N}} df_l' \\ = & \frac{2}{\pi f_D'} \int_0^{f_D'} \frac{\cos\left(\frac{2\pi(n_1-n_2)f_l'T_f}{N}\right)}{\sqrt{1-\left(f_l'/f_D'\right)^2}} df_l'. \end{aligned} \tag{2.34}$$

Employing some manipulations together with the integral representation of the zeroth-order Bessel function of the first kind [31], we have

$$\begin{aligned} E\left\{e^{\frac{j2\pi\epsilon_l(n_1-n_2)}{N}}\right\} &= J_0\left(\frac{2\pi\left(n_1-n_2\right)f_D'T_f}{N}\right) \\ &= J_0\left(\frac{2\pi\left(n_1-n_2\right)\epsilon_D}{N}\right). \end{aligned} \tag{2.35}$$

Therefore, we formulate the ICI variance as

$$\sigma_{ICI}^2 = E_s \sum_{\substack{k=0 \\ k\neq m}}^{N-1} E\left\{C_{m,k}C_{m,k}^*\right\} \tag{2.36}$$

$$= \frac{E_s}{N^2} \sum_{\substack{k=0 \\ k\neq m}}^{N-1} \sum_{n_1=0}^{N-1} \sum_{n_2=0}^{N-1} \phi_t\left(n_1-n_2\right) e^{\frac{-j2\pi(m-k)(n_1-n_2)}{N}} J_0\left(\frac{2\pi\left(n_1-n_2\right)\epsilon_D}{N}\right) \tag{2.37}$$

$$= \frac{E_s}{N^2} \sum_{n_1=0}^{N-1} \sum_{n_2=0}^{N-1} \phi_t\left(n_1-n_2\right) J_0\left(\frac{2\pi\left(n_1-n_2\right)\epsilon_D}{N}\right) e^{\frac{-j2\pi m(n_1-n_2)}{N}} \sum_{\substack{k=0 \\ k\neq m}}^{N-1} e^{\frac{j2\pi k(n_1-n_2)}{N}}.$$

Finally, the ICI variance is written as

$$\sigma_{ICI}^2 = \frac{E_s(N-1)\phi_t\left(0\right)}{N} - \frac{2E_s}{N^2} \sum_{\Delta n=1}^{N-1} \left(N-\Delta n\right) \Re\left\{J_0\left(\frac{2\pi\epsilon_D\Delta n}{N}\right)\phi_t\left(\Delta n\right)\right\}, \tag{2.38}$$

where $\Delta n = n_1 - n_2$. Note that the ICI variance is independent of the subcarrier index m. Thus, according to Eq. (2.38), the ICI statistics is subcarrier-independent. Since the maximum Doppler frequency f'_D is normalized by the OFDM symbol duration T_f, the ICI variance is independent of the absolute Doppler frequency values. Figure 2.3 shows the ICI variances, σ^2_{ICI}, versus the *maximum OFDM symbol normalized Doppler frequency*, ϵ_D, where the Jake's model in [28] is adopted in the simulation.

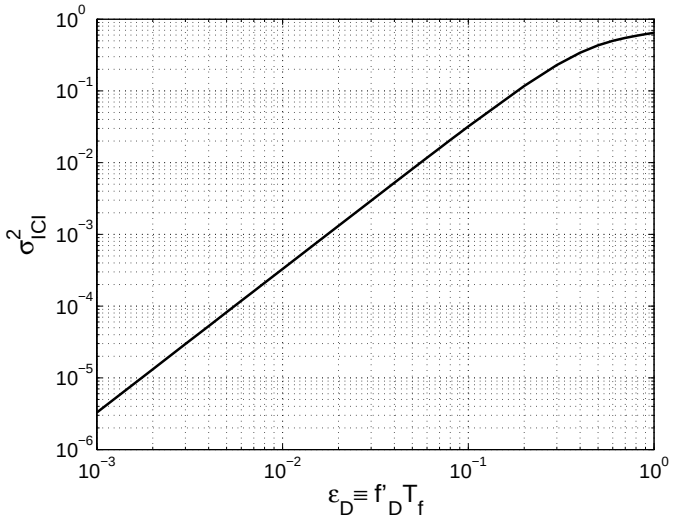

Figure 2.3: ICI Variances

According to Figure 2.3, for the Jake's model, the *maximum OFDM symbol normalized Doppler frequency* must be less than 0.05 rather than 0.08 as claimed in [23] to achieve the SIR=20 dB or larger. It results from that the analysis in [23] did not consider the multiple Doppler frequency shifts in the time-varying multipath channels.

To better understand the Doppler effect on the OFDM systems, Table 2.1 lists the

Table 2.1: Doppler frequency

System	$f_c(Hz)$	T(μs)	f'_D (Hz)	ϵ_D
DVB-T	750M	1194.667*	69.5	0.083
802.11a[10]	5G	4	463.3	0.0019
802.16a[11]	2G-6G	12.8	185.3-556	0.0024-0.0071
UMTS[32]	2G	471.9	185.3	0.0875
HIPERLAN[33]	17G	51.2	1575.3	0.0807
WATM**	60G	2.3	5560	0.0128

*[9] 8K mode in 6MHz bandwidth.
** WATM (Wireless Asynchronous Transfer Mode) system parameters follow the specifications of the Advanced Communications Technologies and Services (ACTS) Median System.

maximum Doppler frequencies f'_D and the corresponding *maximum OFDM symbol normalized Doppler frequencies* ϵ_D for the mobile OFDM receiver at a speed of $100km/hr$ or $27.8m/s$.

In order to further simplify the ICI coefficient matrix, we will investigate the variances of the entries in $\tilde{C}$. Substituting Eq. (2.35) into Eq. (2.33) and setting $k = m$, we obtain

$$\begin{aligned} E\left\{|\, \alpha_m \,|^2\right\} &= E\left\{|\, C_{m,m} \,|^2\right\} \quad 0 \le m \le N-1 \\ &= \frac{1}{N} + \frac{2}{N^2} \sum_{\Delta n=1}^{N-1} (N - \Delta n)\, \Re\left\{\phi_h(\Delta n)\, J_0\left(\frac{2\pi\epsilon_D \Delta n}{N}\right)\right\}. \end{aligned} \tag{2.39}$$

Note that $E\{|\, C_{m,m} \,|^2\}$ is not a function of the subcarrier index m or it is subcarrier-independent. In addition, we obtain

$$\begin{aligned} & E\left\{|\, C_{m,k} \,|^2\right\} = E\left\{C_{m,k}, C^*_{m,k}\right\}, \quad 0 \le m, k \le N-1 \\ = \; & \frac{1}{N} + \frac{2}{N^2} \sum_{\Delta n=1}^{N-1} (N - \Delta n) \Re\left\{e^{\frac{-j2\pi(m-k)\Delta n}{N}} J_0\left(\frac{2\pi\epsilon_D \Delta n}{N}\right) \phi_h(\Delta n)\right\}. \end{aligned} \tag{2.40}$$

It is noted that $E\{|\, C_{m,k} \,|^2\}$ is a function of the subcarrier offset $m-k$. Figure 2.4 depicts $E\{|\, C_{m,k} \,|^2\}$ normalized by $E\{|\, C_{m,m} \,|^2\}$ as a function of $m-k$, where the number of subcarriers is $N = 256$ and different *maximum OFDM symbol normalized Doppler frequency*

values are considered. According to Figure 2.4, it can be found that as the *maximum OFDM symbol normalized Doppler frequency* increases, more and more neighboring subcarriers are involved to interfere the subject subcarrier. Figure 2.5 illustrates how many adjacent subcarriers are actually involved to cause the ICI in percentage. Perceivably, the ICI power tends to concentrate in the neighborhood of the subject subcarrier. When the *maximum OFDM symbol normalized Doppler frequency* is as large as 0.8, 12 neighbour subcarriers contribute as much as 95% of the total ICI power. In other words, the remote subcarriers, which are far away from the subject subcarrier, cause much less ICI, i.e., $|C_{m,k_1}|^2 > |C_{m,k_2}|^2$ if $(|m-k_1|)_N < (|m-k_2|)_N$ for any $0 \leq m, k_1, k_2 \leq N-1$ and $k_1, k_2 \neq m$, where $(i)_N$ is the modulo-N operator.

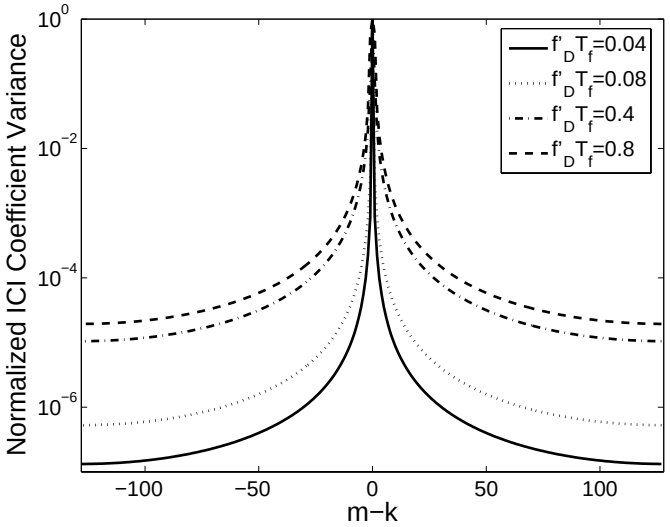

Figure 2.4: ICI coefficient variance

According to Figure. 2.4 and Figure. 2.5, the ICI power decreases significantly as $|m-k|$ decreases. And the ICI arises from just a few adjacent subcarriers even if the

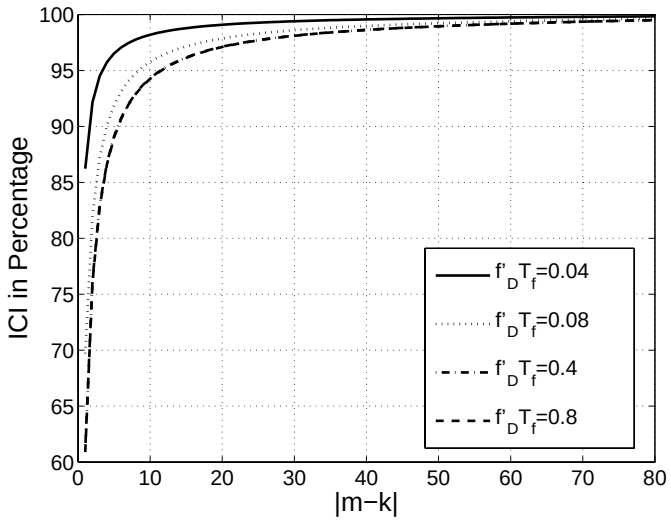

Figure 2.5: Number of subcarriers involved in ICI

maximum Doppler frequency shift is high. Therefore, it is inefficient to build an ICI equalizer involving all subcarriers since the interferences to the subject subcarrier mostly comes from very few neighbouring subcarriers. This is the motivation for us to design an efficient equalizer in this dissertation.

To conclude our new ICI analysis for time-varying multipath channels in the presence of multiple Doppler frequencies in this section, we provide the OFDM system performances based on the Monte Carlo simulations in terms of the average SIR over all subcarriers and the symbol error rate (SER) in different conditions.

The SIR for the mth subcarrier is given by $SIR_m = \frac{|\alpha_m|^2 E_s}{\sigma^2_{ICI}}$. Given the ICI variance defined by Eq. (2.38), and α_m defined by Eq. (2.39), the exact SIR for each subcarrier could be calculated. The average SIR is $\frac{1}{N}\sum_{m=0}^{N-1} SIR_m$. Figure 2.6 illustrates the average SIRs obtained from the Monte Carlo simulation and the exact calculation. The simulation parameters are chosen as follows. The number of subcarriers is $N = 512$ and the length of

cyclic prefix is $G = 64$. We simulate a WSSUS channel according to the COST207 model for typical urban areas in [34]. Each channel tap is a complex-valued Gaussian random process which is independently generated according to the Jakes' Doppler spectrum. The Doppler frequency shift for each path is independently randomized with the probability density function given in Eq. (2.20) between $-f'_D$ and f'_D.

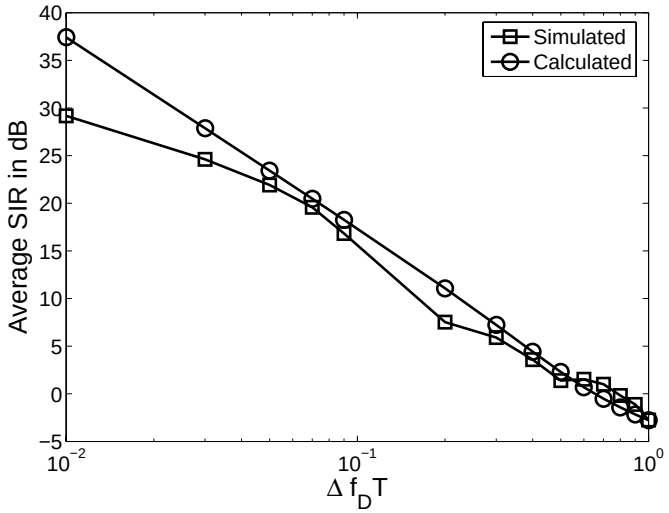

Figure 2.6: Average SIR versus ϵ_D

It is obvious that as the maximum Doppler frequency increases, the average SIR decreases and the OFDM system performance will degrade dramatically. The following simulations will demonstrate this phenomenon. In the following simulations, we assume that the OFDM receiver employs a one-tap equalizer to perform the coherent detection. The one-tap equalizer is designed using the complete knowledge about the channel. The SERs versus the *maximum OFDM symbol normalized Doppler frequency* ϵ_D for different AWGN variances are investigated. The signal-to-noise ratio (SNR) is defined as $\frac{E_s}{\sigma_w^2}$ with

the AWGN variance σ_w^2. Figure 2.7 and Figure 2.8 present the simulated SERs versus the *maximum OFDM symbol normalized Doppler frequency* for the QPSK- and 16QAM-OFDM systems respectively when the variances of the additive white Gaussian noise vary. Finally, a set of simulations are conducted when the *maximum OFDM normalized Doppler frequency* is fixed to 0.06 and the SNR varies from 0 to 40 dB. Figure 2.9 shows the SERs for the QPSK- and 16QAM-OFDM systems. According to these figures, as the *maximum OFDM symbol normalized Doppler frequency* increases, both OFDM system performances degrade dramatically. Higher-order modulation schemes such as 16QAM appear to suffer more from the ICI than lower-order modulation schemes such as QPSK. Time-varying channels impose a severe limitation on the OFDM quality-of-service in terms of SERs. An irreducible error probability floor about 10^{-2} for QPSK-OFDM and 10^{-1} for 16QAM-OFDM would arise. In reality, as the OFDM symbol period and the carrier frequency increase in fast-moving mobile OFDM transceivers, the time-varying multipath channel together with the Doppler effect will be the severe problem for OFDM systems.

2.4 Summary

In this chapter, we first established the OFDM system transmission model based on the adopted channel model. Then we derived a mathematical framework for the OFDM systems in the fast time-varying fading channels in the presence of multiple Doppler frequency shifts. An ICI expression was derived from the underlying system model. According to the simulation results, the OFDM system performance will suffer from an irreducible error probability floor in the fast time-varying fading channels. The conventional assumption

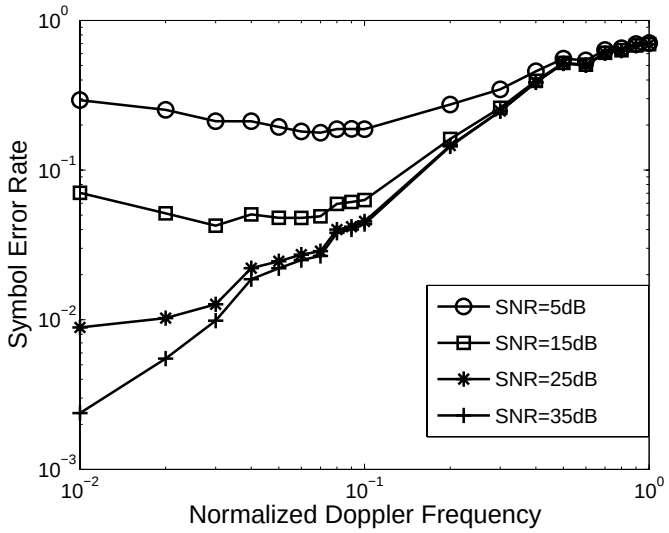

Figure 2.7: SER for QPSK OFDM

for the OFDM system that the channel variations are negligible during one OFDM symbol block no longer holds. Therefore, new algorithms are in demand to combat the ICI in the fast time-varying channels. We observed from the simulation results that the ICI power mostly comes from a few adjacent subcarriers. This motivates our proposed Q-tap equalizer later on. Rather than involving all subcarriers to equalize the subject subcarrier signal, we will employ only a few adjacent subcarriers in our new equalizer. Our new approach will be investigated in detail in Chapter 4. Prior to the introduction of our proposed algorithm, the previous work related to the ICI mitigation in OFDM are discussed in Chapter 3.

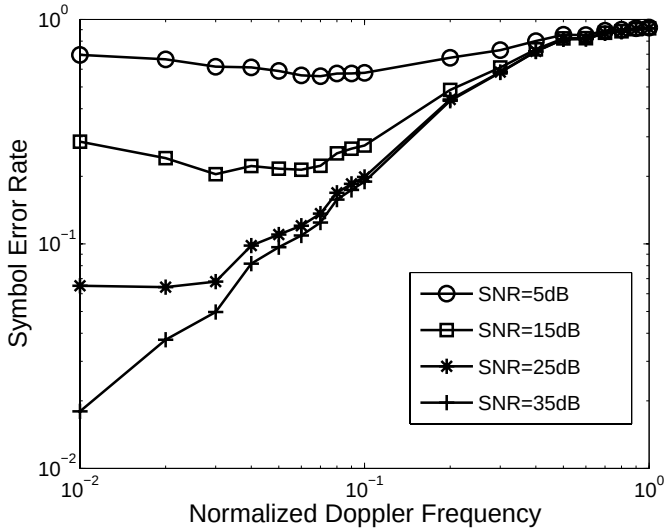

Figure 2.8: SER for 16QAM OFDM

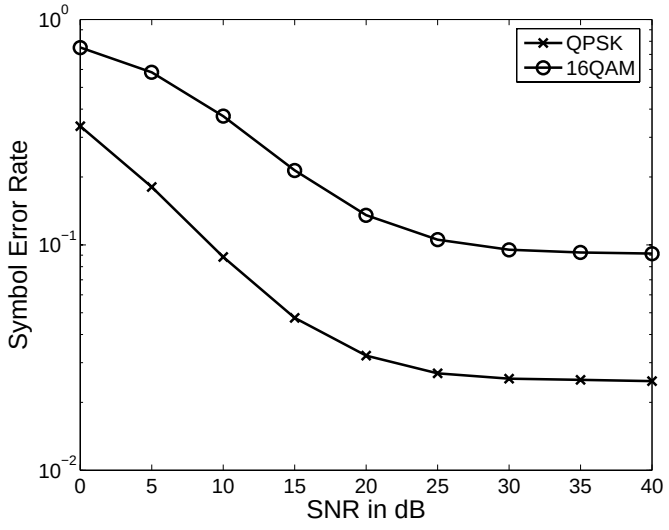

Figure 2.9: SER for QPSK/16QAM Modulations

Chapter 3

Previous Work on ICI Mitigation

In order to mitigate ICI due to the fast time-varying fading channels, three types of approaches have been proposed in the existing literature. The first approach is the ICI equalization, in which the ICI mitigation is achieved via two steps, namely *channel estimation* and *ICI removal* [35]-[52]. The second approach is the pre-processing either through the windowing or the coding [19][20][53]-[59], which reduces the sensitivity of the OFDM performance to the time- and frequency- selective channels. The third approach utilizes the space-time diversity provided by the multiple transmitting and receiving antennae [60][61]. The outline of this section can be stated as follows. Section 3.1 provides an overview for the first approach. The algorithms using the second approach are introduced in section 3.2. Finally, the introduction of the third approach will be presented in Section 3.3.

3.1 Approach 1

The techniques using the first approach require neither any modification in the transmitter so that they are compatible with existing standards unlike some precoding techniques in the second approach nor any additional hardware as the techniques using the third approach based on multiple transmitting and receiving antennae [35]-[61]. In recent years, considerable research has been devoted to the time-varying channel estimation for OFDM system [35]-[52]. These channel estimation algorithms can be categorized as the model-free channel estimation [25][35]-[42] and model-based channel estimation [43]-[46].

The model-free channel estimation relies only on knowledge of the received signal together with some *a prior* statistical information about the channel, while the model-based channel estimation depends on the predefined mathematical formulation for the time-varying channels [43]-[46]. The underlying channel parameters rather than the CIR are to be estimated at the receiver in the model-based channel estimation [43]-[46]. After the channel estimation, the ICI can be removed either using a decision-feedback equalizer [4] or using a least-square (LS) or minimum-mean-square-error (MMSE) equalizer [4]. Next we will discuss the channel estimation algorithms and the ICI removal techniques.

3.1.1 Channel Estimation

First, we will focus on the model-free channel estimation. The channel estimations in [25][35] were achieved by regularly inserting pilot symbols in the OFDM symbol stream. Specifically, the training sequence was a Dirac-delta function consisting of only one non-trivial data sample which was surrounded by two subsequences of zero values each with the identical sequence length to that of the cyclic prefix. The complete channel estimation for one OFDM symbol can be achieved by using a linear interpolation based on the assumption that the channel varies in a linear fashion within an OFDM symbol duration [25]. In [36], an MMSE channel estimator with the aid of the dedicated OFDM training symbols employed in the context of decision-directed channel estimation was proposed. Unlike in [25][35], channel was assumed to vary linearly during a few OFDM symbol duration instead of one OFDM symbol duration in [37]. Based on the pilots inserted into every OFDM symbol, a

maximum-likelihood (ML) channel estimator was derived. Also according to the observation that the direct ML channel estimate is close to the real channel in the middle time instant of an OFDM symbol duration; three consecutive OFDM symbols are involved in the corresponding channel estimation; the channel estimation at the middle time instant are linearly interpolated to estimate the real channel [37]. However, the assumption that channel varies linearly usually does not hold when the OFDM symbol normalized Doppler frequency is large [25].

In [38], the CIR $h(n, l)$ was estimated using a linear combination of pilot symbols based on the MMSE criteria at the receiver. In their channel estimation scheme, all subcarriers in some few OFDM symbols are all allocated as pilot symbols while in most of time, OFDM symbols consist of information data only. A reduced-complexity MMSE estimator was also proposed in [38] using the optimal rank-reduction [62]. This technique requires *a priori* knowledge of the channel statistics. Although this scheme can work without the precise channel statistics, its performance is significantly degraded if the assumed Doppler frequency is lower than the actual value.

It was observed that the wireless radio channel can be parameterized as a combination of paths, each characterized by a delay and a complex-valued amplitude. The amplitude for each path illustrates fast temporal variations due to the mobility of terminals while the delays are almost constant over a large number of OFDM symbols [39]. A technique which tracks the delay-subspace by a subspace tracking algorithm and estimates the amplitudes via the least-mean-square algorithm was proposed [39].

Instead of estimating the CIR $h(n,l)$ directly using the aforementioned methods, we can also employ the following algorithms to estimate the ICI coefficient matrix $C_{m,k}$ using the pilot symbols. In [40], a novel OFDM channel estimation algorithm based on comb-type of groups of pilot symbols can be found. There are two crucial assumptions associated this proposed algorithm [40]. Usually, the size of matrix $\tilde{C}$ is very large since there are many subcarriers in every OFDM symbol. For reducing the number of parameters to be estimated in $\tilde{C}$, we can make the first assumption that only a few neighboring subcarriers contribute to the dominant ICI to interfere the subject subcarrier. The second assumption is that the diagonal element $\alpha_m, 0 \leq m \leq N-1$, in the ICI coefficient matrix $C_{m,k}$ are correlated with each other, and the elements on off-diagonals, $C_{m,k}, 0 \leq m,k \leq N-1$, with $m-k = constant$ are also correlated with each other. Thus, the ICI coefficients can be estimated using an interpolation based on the pilot symbols. The diagonal and off-diagonal correlations are determined by using the channel statistics [40].

Among all the aforementioned model-free channel estimation algorithms, pilot symbols are always needed. In [42], five different pilot symbol patterns were investigated for channel estimation and compared in terms of bit error rates. The capability of estimating the channel with high mobility reliably depends on the adopted pilot symbol pattern [42]. The pilot symbols are supposed to spread out both in time and frequency domains [42].

For model-based channel estimators, time-varying channel are approximated by some

mathematical models [43]-[46]. In [43], the channel variations of each path were approximated by using a linear model with a constant slope in an OFDM symbol and the least-square estimator of the CIR was obtained by inserting equispaced pilot symbols in every OFDM symbol. In [44], the channel was modeled by expanding each path attenuation factor $\gamma(t, l)$ into a Taylor series as a function of t around the middle time instant of an OFDM symbol, namely $t = \frac{T}{2}$, where $t = 0$ corresponds to the first time sample at the input of the OFDM demodulator. In this scheme, the channel time derivatives in the Taylor series instead of CIR were estimated and multistage estimation scheme was proposed, which estimates the higher-power derivatives while modeling the lower-power derivatives as the white noise. Consequently, the ICI coefficient matrix $\tilde{C}$ can be derived as a function of the channel time derivatives [44]. Similarly in [45], the time-varying channel frequency responses was modeled using a finite power series expansion. The channel estimation is achieved with the *a priori* statistical properties of the channel. The proposed channel estimation method in [45] uses the pilot symbols and statistical characterization of time and Doppler spread based on Jakes model for designing a maximum-likelihood estimator. Alternatively, a new OFDM channel estimator based on the modified Kalman filter (MKF) for a fast-changing frequency-selective Rayleigh fading environment was proposed in [46]. The time-varying channel is modeled as an autoregressive (AR) process and the proposed MKF is applied to estimate the AR parameters [46].

3.1.2 ICI Removal

In the first ICI equalization approach, once the channel information is obtained at the receiver, a zero-forcing (ZF) equalizer, or an MMSE equalizer was proposed in [25][36] and [47] respectively. All the algorithms in [25][36][47] involve a large matrix inversion with high computational complexity. To reduce such computational complexity, the "small" ICI coefficients in the ICI coefficient matrix $\tilde{C}$ are ignored [25][38]. It is assumed that the channel varies linearly, and the dominant ICI coefficients gather around a small number of neighboring subcarriers. Instead of a direct matrix inversion, a Gauss-seidel iteration algorithm was proposed to simplify it in [48]. Besides, a jacobi stationary iterative algorithm was also proposed to compensate the ICI terms in [49]. Such a proposed algorithm utilized the properties of the Toeplitz and the Fourier matrices to obtain the intercarrier interference terms in the frequency domain with low complexity based on the linearly varying channel assumption.

To deal with the disadvantage of noise amplification in the ZF equalizers [4], which causes the system performance degradation when there exist deep nulls in the channel frequency response, a novel ZF equalizer for OFDM over time- and frequency- selective channels using the existing frequency-domain redundancy was proposed in [43][50]. In many OFDM-related standards, several null carriers are appended to provide guard bands, where those null carriers are regarded as the frequency-domain redundancy.

Unlike the aforementioned MMSE and ZF equalizers which require large matrix inversions, a two-stage equalizer with symbol estimation strategies for OFDM in the presence

of doubly-selective fading was proposed in [51] and an iterative decision-feedback equalizers were employed to remove the ICI in [35][38][52]. For the two-stage equalization scheme [51], at the first stage, rather than simply ignoring small-valued ICI coefficients as in [25][38], the authors used a signal-to-interference-plus-noise ratio (SINR) optimal low-complexity linear preprocessing (windowing) to "squeeze" the ICI into a few coefficients; then at the second stage, the authors proposed a low-complexity iterative symbol estimation scheme that leverage the ICI-shortened channel representation. Combining the techniques in [25] and [38], the authors in [52] derived the recursive algorithms to remove the ICI. It has been showed in [52] that time-varying channel leads to the narrowly-distributed symbol energy over a few subcarriers and the ICI power on a subcarrier is mainly contributed by a few neighboring subcarriers. Based on this fact, a low-complexity MMSE and decision-feedback equalizer for ICI suppression were proposed in OFDM receivers [52]. A universal lower bound on the partial ICI power was derived when $f'_D T < 1$, which shows that more than 90% of the ICI power comes from 12 neighboring subcarriers. It has also been shown that most of the symbol energy is distributed over a few subcarriers. That is, when $f'_D T = 0.3$, more than 90% of the symbol energy spreads over only three subcarriers. Accordingly, the development of low-complexity MMSE and DFE receivers for ICI suppression were motivated in [52].

Another two-stage decision-feedback scheme called DF-ICI was proposed in [44][45]. Initially, a standard equalizer, namely a one-tap filter for each subcarrier, is applied. The tentatively detected data is used to regenerate the ICI, which is then subtracted from the

received signal. Some drawbacks of the DF-ICI in [45] were relieved in [44], the algorithm in [45] adopted an iterative ICI cancellation and channel estimation scheme. The ICI is canceled iteratively, where at every stage the transmitted signal can be estimated more and more reliably.

3.2 Approach 2

Compared to previously described equalization approach, the windowing and precoding method using the second approach have two major advantages [19][20][53]-[59]. The first advantage is its low complexity. In the equalization approach, the channel estimation and ICI removal always involve heavy computations. However, in the windowing/precoding techniques, usually simple algorithms are involved at transceivers. The second advantage is that no CIR estimation is needed dynamically to estimate the time-varying channels. The windowing and precoding schemes do not require the specific channel estimation. Instead, they are simply designed to mitigate the ICI [19][20].

A simple and effective precoding method, the ICI self-cancellation scheme was proposed in [19][20], where a polynomial coding in the frequency domain was used to mitigate the frequency offset effect. In the ICI self-cancellation method, one information symbol was duplicated for a group of P adjacent subcarriers using a group of weighting coefficients. The weights were designed such that at the receiver, the ICI was minimized in the presence of the channel frequency errors. Empirically, this method significantly reduces the ICI in the trade-off of the spectral efficiency reduction with a factor of P. In [19][20], the ICI self-cancellation coding rate was one half with $P = 2$. In general, the ICI self-cancellation

coding rate can be set as $1/P$ with the weights chosen as the coefficients of the polynomial $(1-D)^P$ as stated by [53]. Therefore, the ICI self-cancellation is also known as the polynomial cancellation coding (PCC). A rate $(P-1)/P$ precoder was proposed in [54] by modifying the previous rate 1/2 precoder [20][53]. The new precoder in [54], which extended the half-rate precoder in [20][53] and, was based on two assumptions. First, the magnitudes of the diagonal elements α_m in the ICI coefficient matrix $\tilde{C}$ are considerably larger than those of the off-diagonal elements. Second, the magnitudes of any two neighboring off-diagonal elements of $\tilde{C}$ are close to each other. A special case of the new precoders in [54] with rate 2/3 was also developed in [55]. To improve the system performance, Turbo product coding was integrated with half-rate ICI self-cancellation precoder in [56]. The ICI self-cancellation scheme can also be achieved using the time-domain windowing in transceivers, which was proposed in [57]. In the self-cancellation method [19][20], the same information symbol is modulated on P adjacent subcarriers with the pre-defined weighting coefficient. This leads to a reduction of ICI since the sum of ICI interferences that these P subcarriers generate on another subcarrier is very small. In the frequency domain, the sum of the signals of these P subcarriers has a shape that has approximate nulls around the location of other subcarriers, and, therefore, leads to less ICI. The proposed windowing scheme shapes the subcarrier signal spectra that creates less ICI using a windowing operation in the time domain. It has been shown that the ICI self-cancellation method in [19][20] is equivalent to special cases of the proposed scheme [57]

We will provide an introduction of the precoders to mitigate the ICI, which have also

been adopted in our work. The OFDM demodulated signal as given by Eq.(2.28) with a precoder can be expressed as

$$\begin{aligned} \vec{Y} &= \tilde{C}\vec{X} + \vec{W} \\ &= \tilde{C}\tilde{\Gamma}\vec{d} + \vec{W}, \end{aligned} \tag{3.1}$$

where $\tilde{\Gamma}$ is a precoder matrix, and $\vec{d}$ is the information symbol vector. $\tilde{\Gamma}$ is of size N-by-$N \times R$, where R is the coding rate, and N is the number of subcarriers in OFDM. For example, if $N = 4$, a half-rate precoder matrix in [20] is given by

$$\tilde{\Gamma} = \frac{1}{\sqrt{2}} \begin{bmatrix} 1 & 0 \\ -1 & 0 \\ 0 & 1 \\ 0 & -1 \end{bmatrix}. \tag{3.2}$$

According to [54], the precoder matrix $\tilde{\Gamma}$ can be generated as follows:

1. $\tilde{\Gamma}$ is the block diagonal matrix with identical blocks, i.e. $\tilde{\Gamma} = diag\{\tilde{B}, \tilde{B}, ..., \tilde{B}\}$, where block $\tilde{B}$ is an a-by-b matrix, and the coding rate R can be expressed as $R = \frac{b}{a}$. For example $\tilde{B} = \sqrt{1/2}[1 \ -1]^T$ as defined by [20].

2. The rank of $\tilde{B}$ is b.

3. The trace of $\tilde{B}\tilde{B}^T$ is equal to a.

4. All column vectors in $\tilde{B}$ have only two non-zero elements at two consecutive rows, and those two elements are summed to be zero.

For example, the following matrix $\tilde{B}$ satisfies the above-mentioned conditions such that

$$\tilde{B} = \sqrt{\frac{2}{3}} \begin{bmatrix} 1 & 0 & 0 \\ -1 & 1 & 0 \\ 0 & -1 & 1 \\ 0 & 0 & -1 \end{bmatrix}. \tag{3.3}$$

To avoid the previously described spectral efficiency sacrifice, a frequency-domain precoder known as partial response coding (PRC) with rate one (full spectral efficiency) was proposed in [58][59]. The PRC in conjunction with maximum-likelihood sequence detection to mitigate ICI in OFDM systems was investigated in [58].

3.3 Approach 3

Multi-input multi-output (MIMO) systems adopt multiple antenna array for wireless transceivers. Many techniques which have been applied to the MIMO systems in both space and time domains can effectively increase the system capacity and improve the reliability of wireless link [63]. On the other hand, the OFDM technology has been widely used in wireless multimedia communications, due to its high data transmission rate, high bandwidth efficiency and excellent performance in resisting multipath fading channels [13]. By integrating OFDM systems with MIMO techniques and introducing space-time diversities, we can simultaneously enhance both communications capacity and performance [64].

To further improve the MIMO-OFDM performance in mobile communications, a training-sequence design scheme with high bandwidth efficiency, and an iterative least-square (LS) channel estimation algorithm were proposed in [60]. Using a lowpass filter

to reduce the ICI significantly, this LS algorithm can estimate channel state information accurately [60].

A bank of LTV (Linear Time-Variant) filters which maximize the signal-to-ICI-plus-noise energy ratio was designed in [61]. Then the filtering-based ICI mitigation technique was proposed where such a bank of filters follow the time-varying channel so the overall system model is approximately time-invariant. The techniques using the third approach may require high hardware cost, since multiple receiver antennae may be in demand.

In summary, we would like to focus on the first and the second approach in this dissertation since the first approach does not require any modification in the transmitter so that it is compatible with the existing standards, while the second approach is computationally efficient compared with the first approach, and its hardware cost is minimum compared with the third approach. Chapter 4 is dedicated to design a channel estimator and an equalizer using the first approach to mitigate the ICI. A proposed alternative algorithm using the second approach is based on the ICI self-cancellation coding, which will be described in Chapter 5.

Chapter 4

Proposed ICI Mitigation Algorithm

According to the analysis in Chapter 2, the time variations of the channel within one OFDM symbol block in the presence of multiple Doppler frequency shifts destroy the subcarrier orthogonality, result in the ICI and hence lead to an irreducible error probability floor when only a one-tap equalizer is employed. The performance degradation due to the ICI becomes significant as the carrier frequency, the OFDM symbol duration and vehicular velocity increase. As shown in Chapter 3, the first approach involving an equalizer is effective for the ICI mitigation. However, the designs of the traditional MMSE, ZF equalizers for OFDM systems in [25][36][47] normally require a large matrix inversion. Several algorithms in [25][38][48][49] were developed to reduce the computational complexity of this huge matrix inverse. Moreover, all these schemes in [25][36][38][47][48][49] equalize N subcarrier signals simultaneously using the N available received signals in one OFDM symbol block. However, the ICI coefficient matrix $\tilde{C}$ becomes very large when N is large, for example, $N = 1024$ in the standard WMAN systems in [11]. Therefore, any straightforward implementation of a traditional MMSE or ZF equalizer should be avoided. It has also been shown in Chapter 2 that the ICI power is concentrated only on a few adjacent subcarriers. In other words, the subject subcarrier would be interfered only by a few neighbors. Accordingly, the computational complexity of the ICI equalizer can be reduced significantly without the significant performance sacrifice. In this chapter, a new approach using the Q-tap equalizer integrated with a MMSE ICI coefficient estimator is introduced

for the frequency-domain ICI equalization and channel estimation, and the simulation results are also presented to show the effectiveness of our proposed method. This chapter is organized as follows. Section 4.1 is dedicated to the new Q-tap equalizer, which includes both Minimum Mean Square Error (MMSE) linear equalizer and Decision Feedback (DF) non-linear equalizer. In Section 4.2, we introduce a new ICI coefficient estimation algorithm which employs the Wiener filtering based on the channel correlation properties in both time and frequency domain. Based on the simulation results of our proposed ICI mitigation algorithm, the conclusion will be drawn in Section 4.3.

4.1 ICI Mitigation Equalizer

Similar to the first approach described in Chapter 3, our proposed ICI mitigation algorithm includes two steps. At the receiver, the channel is first estimated, and then an equalizer is employed to suppress the ICI. This section is focused on the design of such an equalizer, under the assumption that the ICI coefficient matrix $\tilde{C}$ is given. The estimation of the ICI coefficient matrix $\tilde{C}$ will be studied in Section 4.2. Since the ICI arises from a few neighboring subcarriers, Q-tap equalizers, which reduce the computational complexity, are proposed. In this section, two Q-tap equalizers, namely linear MMSE equalizer and non-linear DF equalizer, are investigated. The rest of this section is organized as follows. The linear MMSE Q-tap equalizer and nonlinear DF Q-tap equalizer are discussed in Sub-section 4.1.1 and Sub-section 4.1.2, respectively. The computer simulation results for these two equalizers are presented in Sub-section 4.1.3. Sub-section 4.1.4 will draw the concluding remarks on the proposed Q-tap MMSE and DF equalizers.

4.1.1 Q-tap Minimum Mean Square Error (MMSE) Equalizer

In this sub-section, we design a Q-tap MMSE equalizer using the mathematical framework developed in Chapter 2. First, the traditional MMSE equalizer approached is introduced. Then with further modifications, we can design a Q-tap MMSE equalizer.

The conventional OFDM receiver operation using a one-tap equalizer exhibits relatively good performance when the *maximum OFDM symbol normalized Doppler frequency shift* is small. However, in the environment where the *maximum OFDM symbol normalized Doppler frequency shift* is high, the orthogonality among subcarriers does not exist, and there is an irreducible error probability floor due to the ICI. We will show how to design this Q-tap MMSE equalizer to mitigate the ICI. Invoke the OFDM system model in Eq. (2.28)

$$\vec{Y} = \tilde{C}\vec{X} + \vec{W}. \tag{4.1}$$

It is assumed that the ICI coefficient matrix $\tilde{C}$ can be estimated. The traditional MMSE equalizer, which is an N-by-N matrix $\tilde{G}$, is a matrix which minimizes the cost function $E\left\{\| \vec{X} - \hat{\vec{X}} \|^2\right\}$, where $\hat{\vec{X}} = \tilde{G}\vec{Y}$ is the equalizer output vector. Thus, it yields

$$\tilde{G} = \tilde{R}_{\vec{X}\vec{Y}}\tilde{R}^{-1}_{\vec{Y}\vec{Y}}, \tag{4.2}$$

where $\tilde{R}_{\vec{X}\vec{Y}}$ denotes the correlation matrix between $\vec{X}$ and $\vec{Y}$, defined as $\tilde{R}_{\vec{X}\vec{Y}} \equiv E\left\{\vec{X}\vec{Y}^H\right\}$ and $\tilde{R}_{\vec{Y}\vec{Y}}$ is the correlation matrix of $\vec{Y}$, defined as $\tilde{R}_{\vec{Y}\vec{Y}} \equiv E\left\{\vec{Y}\vec{Y}^H\right\}$. Here $()^H$ denotes the complex-conjugate transpose. The resulting mean-squared error (MSE) is given by

$$MSE = tr\left(\tilde{R}_{\vec{X}\vec{X}} - \tilde{R}_{\vec{X}\vec{Y}}\tilde{R}^{-1}_{\vec{Y}\vec{Y}}\tilde{R}_{\vec{Y}\vec{X}}\right), \tag{4.3}$$

where $\tilde{R}_{\vec{X}\vec{X}} \equiv E\left\{\vec{X}\vec{X}^H\right\}$, $\tilde{R}_{\vec{Y}\vec{X}} \equiv E\left\{\vec{Y}\vec{X}^H\right\}$, and $tr(\cdot)$ denotes the trace operator. Given that $\tilde{C}$ is known and $\vec{X}$ is a zero-mean i.i.d random vector with the variance σ_X^2, and $\vec{W}$ is a zero-mean AWGN vector with a variance σ_W^2 ($\vec{W}$ is independent of $\vec{X}$), $\tilde{R}_{\vec{X}\vec{Y}}$ becomes

$$\begin{aligned} \tilde{R}_{\vec{X}\vec{Y}} &= E\left\{\vec{X}\vec{Y}^H\right\} \\ &= E\left\{\vec{X}\left(\tilde{C}\vec{X}+\vec{W}\right)^H\right\} \\ &= E\left\{\vec{X}\vec{X}^H\right\}\tilde{C}^H + E\left\{\vec{X}\vec{W}^H\right\} \\ &= \sigma_X^2\tilde{C}^H, \end{aligned} \tag{4.4}$$

and $\tilde{R}_{\vec{Y}\vec{Y}}$ is

$$\begin{aligned} \tilde{R}_{\vec{Y}\vec{Y}} &= E\left\{\vec{Y}\vec{Y}^H\right\} \\ &= E\left\{\left(\tilde{C}\vec{X}+\vec{W}\right)\left(\tilde{C}\vec{X}+\vec{W}\right)^H\right\} \\ &= \tilde{C}E\left\{\vec{X}\vec{X}^H\right\}\tilde{C}^H + E\left\{\vec{W}\vec{W}^H\right\} \\ &= \sigma_X^2\tilde{C}\tilde{C}^H + \sigma_W^2\tilde{I}_N, \end{aligned} \tag{4.5}$$

where $\tilde{I}_N$ is the N-by-N identity matrix. The MMSE equalizer in Eq. (4.2) can be rewritten as

$$\tilde{G} = \tilde{C}^H\left(\tilde{C}\tilde{C}^H + \frac{\sigma_W^2}{\sigma_X^2}\tilde{I}_N\right)^{-1}. \tag{4.6}$$

Likewise, the MSE of the equalizer in Eq. (4.3) becomes

$$MSE = \sigma_X^2 tr\left(\tilde{I}_N - \tilde{G}\tilde{C}\right). \tag{4.7}$$

The ZF equalizer can be simply realized when the AWGN is neglected, such that

$$\tilde{G} = \tilde{C}^{-1}, \tag{4.8}$$

which is the inverse of the ICI coefficient matrix $\tilde{C}$. It is well known that such a ZF equalizer experiences more noise enhancement than the MMSE approach when the channel has deep fades. Therefore, we study the MMSE equalizer only here.

According to Eq. (4.6), the MMSE equalizer is too complicated to be implemented, since it involves an N-by-N matrix inverse. N is usually fairly large, for example, $N = 64$ for the IEEE 802.11a standard, $N = 1024$ for the IEEE 802.16 standard, and $N = 2048$ for the DVB standard. The implementation of an MMSE equalizer given by Eq. (4.6) is not feasible. As a matter of fact, the ICI power arises from the neighboring subcarriers around the subject subcarrier, the equalizer complexity can be reduced significantly without much performance trade-off. Consequently, a simplified MMSE equalizer with only Q taps will be investigated in the following.

Instead of employing all subcarriers, we can focus on only a few subcarriers ($(Q-1)/2$ subcarriers) around the subject subcarrier to design an efficient equalizer. For example, if Q is set as 3, two neighboring subcarriers (one on each side) are employed in the simplified equalizer. If the subject subcarrier signal is X_2, then the received signals Y_1, Y_2, Y_3 are all used in the equalizer for a better symbol detection of X_2. Since the ICI coefficient matrix $\tilde{C}$ is circulant in nature, to detect the signal on the 0th subcarrier, the equalizer involves the received signal on the $N-1$th subcarrier.

The derivation of a Q-tap MMSE equalizer is similar to the aforementioned traditional MMSE equalizer. Rather than a huge matrix $\tilde{G}$ involving all subcarriers, we determine the individual equalizer for each subcarrier independently. Let's choose $Q = 2q + 1$. Without

loss of the generality, the Q-tap equalizer coefficients for the mth subcarrier are defined as

$$\vec{g}_m^Q \equiv [g_{-q,m}, g_{-q+1,m}, \cdots, g_{0,m}, g_{1,m}, \cdots, g_{q,m}], \qquad 0 \le m \le N-1, \tag{4.9}$$

which minimizes the mean-square error

$$E\left\{|X_m - \hat{X}_m|^2\right\}, \tag{4.10}$$

where $\hat{X}_m = \vec{g}_m^Q \vec{Y}_m^Q$, and $\vec{Y}_m^Q$ is defined as

$$\vec{Y}_m^Q \equiv [Y_{(m-q)_N}, Y_{(m-q+1)_N}, \cdots, Y_{(m-1)_N}, Y_m, Y_{(m+1)_N}, \cdots, Y_{(m+q-1)_N}, Y_{(m+q)_N}]^T. \tag{4.11}$$

Here $(\cdot)_N$ denotes the modulo operation with modulus N. $\vec{Y}_m^Q$ can then be written as

$$\vec{Y}_m^Q = \tilde{C}_m^Q \vec{X}_m^Q + \vec{W}_m^Q, \tag{4.12}$$

where

$$\vec{W}_m^Q \equiv [W_{(m-q)}, W_{(m-q+1)}, \cdots, W_{(m-1)}, W_m, W_{(m+1)}, \cdots, W_{(m+q-1)}, W_{(m+q)}]^T, \tag{4.13a}$$

$$\vec{X}_m^Q \equiv [X_{(m-2q)}, X_{(m-2q+1)}, \cdots, X_{(m-1)}, X_m, X_{(m+1)}, \cdots, X_{(m+2q-1)}, X_{(m+2q)}]^T, \tag{4.13b}$$

and

$$\tilde{C}_m^Q \equiv \tag{4.13c}$$

$$\begin{bmatrix} C_{(m-q),(m-2q)} & \cdots & C_{(m-q),(m-q)} & \cdots & C_{(m-q),m} & 0 & 0 & \cdots & 0 \\ & \ddots & & \ddots & & \ddots & & \ddots & \\ 0 & \cdots & C_{m,(m-q)} & \cdots & C_{m,m} & \cdots & C_{m,(m+q)} & 0 & \cdots \\ & \ddots & & \ddots & & \ddots & & \ddots & \\ 0 & 0 & \cdots & 0 & C_{(m+q),m} & \cdots & C_{(m+q),(m+q)} & \cdots & C_{(m+q),(m+2q)} \end{bmatrix}_{Q,2Q-1}.$$

Due to the page limit, the modulo-N operator $(\cdot)_N$ is simplified as $(\cdot)$ in Eq. (4.13). Eq. (4.12) results from the ICI coefficient property that $|C_{m,k_1}|^2 > |C_{m,k_2}|^2$ if $(|m-k_1|)_N < (|m-k_2|)_N$ for any $0 \leq m, k_1, k_2 \leq N-1$ and $k_1, k_2 \neq m$, and ICI coefficient $C_{m,k}$ decreases rapidly as $m-k$ increases. Observing both Eq. (4.12) and Eq. (4.1), we can establish the Q-tap equalizer for the mth subcarriers from the aforementioned traditional MMSE equalizer. From Eq. (4.2), the Q-tap MMSE equalizer solution for the mth subcarrier is given by

$$\vec{g}_m^Q = \vec{\eta}_{X_m \vec{Y}_m^Q} \tilde{R}^{-1}_{\vec{Y}_m^Q \vec{Y}_m^Q}. \tag{4.14}$$

Similar to the traditional MMSE equalizer, we have

$$\begin{aligned} \vec{\eta}_{X_m \vec{Y}_m^Q} &= E\left\{ X_m \left(\vec{Y}_m^Q\right)^H \right\} \\ &= E\left\{ X_m \left(\tilde{C}_m^Q \vec{X}_m^Q + \vec{W}_m^Q\right)^H \right\} \\ &= E\left\{ X_m \left(\vec{X}_m^Q\right)^H \right\} \left(\tilde{C}_m^Q\right)^H \\ &= \sigma_X^2 \left[\underbrace{0, 0, \cdots, 0}_{2q}, 1, \underbrace{0, \cdots, 0, 0}_{2q} \right] \left(\tilde{C}_m^Q\right)^H \\ &= \sigma_X^2 (\vec{\nu}_m^Q)^H, \end{aligned} \tag{4.15}$$

where $\vec{\nu}_m^Q$ is the mth column of the matrix $\tilde{C}_m^Q$, i.e.,

$$\vec{\nu}_m^Q = \left[C_{(m-q)_N, m}, C_{(m-q+1)_N, m}, \cdots, C_{m,m}, \cdots, C_{(m+q-1)_N, m}, C_{(m+q)_N, m} \right]^T. \tag{4.16}$$

The vector $\vec{\nu}_m^Q$ corresponds to the truncated version of the mth column in the matrix $\tilde{C}$ by reserving only Q elements centered around the mth row with q rows on either side.

We proceed with the calculation of $\tilde{R}_{\vec{Y}_m^Q \vec{Y}_m^Q}$ in Eq. (4.14). According to Eq. (4.12), we

obtain

$$\begin{aligned}
\tilde{R}_{\vec{Y}_m^Q \vec{Y}_m^Q} &= E\left\{\vec{Y}_m^Q \left(\vec{Y}_m^Q\right)^H\right\} \\
&= E\left\{\left(\tilde{C}_m^Q \vec{X}_m^Q + \vec{W}_m^Q\right)\left(\tilde{C}_m^Q \vec{X}_m^Q + \vec{W}_m^Q\right)^H\right\} \\
&= \tilde{C}_m^Q E\left\{\vec{X}_m^Q \left(\vec{X}_m^Q\right)^H\right\}\left(\tilde{C}_m^Q\right)^H + E\left\{\vec{W}_m^Q \left(\vec{W}_m^Q\right)^H\right\} \\
&= \sigma_X^2 \tilde{C}_m^Q \left(\tilde{C}_m^Q\right)^H + \sigma_W^2 \tilde{I}_Q.
\end{aligned} \tag{4.17}$$

Substituting Eq. (4.15) and Eq. (4.17) into Eq. (4.14), we can achieve the complete Q-tap MMSE equalizer solution as

$$\vec{g}_m^Q = (\vec{\nu}_m^Q)^H \left(\tilde{C}_m^Q \left(\tilde{C}_m^Q\right)^H + \frac{\sigma_W^2}{\sigma_X^2}\tilde{I}_Q\right)^{-1}. \tag{4.18}$$

It is obvious that our proposed Q-tap MMSE equalizer in Eq. (4.18) only involves a Q-by-Q matrix inverse. The corresponding MSE of the Q-tap equalizer, which is given in Eq. (4.18), is

$$MSE = \sigma_X^2 \sum_{m=0}^{N-1} \left(1 - \vec{g}_m^Q \vec{\nu}_m^Q\right). \tag{4.19}$$

If we set Q as small as possible without sacrificing much quality-of-service, we can quite reduce the computational complexity. The full-tap (traditional) MMSE equalizer, which is given in Eq. (4.6), requires an N-by-N matrix inversion with N^3 complex multipliers, while a Q-tap MMSE equalizer needs N sets of Q-by-Q matrix inversions with only NQ^3 complex multipliers. Therefore, using the Q-tap equalizer, the computational complexity in terms of the number of complex multipliers is reduced by $1 - \frac{Q^3}{N^2}$. Note that as N increases, the computational complexity is greatly reduced. For example, when $N = 256$, a 7-tap MMSE equalizer will reduce the computational complexity by almost 99%.

In summary, our proposed Q-tap linear MMSE equalizer is given by Eq. (4.18), which is based on the assumption that the ICI coefficient matrix $\tilde{C}$ is known at the receiver. In the following sub-section, a non-linear Q-tap DF equalizer is also investigated.

4.1.2 Q-tap Decision Feedback (DF) Equalizer

The MMSE equalizer in the previous sub-section is a linear equalizer. However, linear equalization techniques typically suffer from more noise enhancement than nonlinear equalizers [65]. Among nonlinear equalization techniques, the DF equalizers are commonly used, since the corresponding realization is simple and it leads to the promising performance. This sub-section is dedicated to the Q-tap non-linear DF equalizer.

The DF equalizer has been introduced for both channel equalization and multiuser detection [4][66]. In [66], the DF multiuser detection for synchronous code-division multiple-access over Gaussian channels was studied. It has been shown that the DF equalizer outperforms the linear equalizer for every user [66]. Our signal transmission model in Eq. (2.28) is essentially the same as the synchronous CDMA model [66], if we consider that the transmitted signal X_k on the k subcarrier comes from a user k, and the kth column in the ICI coefficient matrix $\tilde{C}$ can be deemed as the spreading code sequence of user k. Generally speaking, we could apply any DF equalizer in [66] for the signal transmission model defined in Eq. (2.28).

In principle, once a transmitted signal has been detected, the interference that it induces on other signals can be estimated and subtracted before the detection of subsequent transmitted signals. The DF equalizer consists of a feedforward filter with the input as the

received signal (similar to the linear equalizer) followed by a feedback filter with the input as the previously detected signal instead. The interference can be characterized as the output of this feedback filter when the detected signal serves as the input. The resulting interference is then subtracted from the received signals. This is the so-called successive interference cancellation scheme.

Our proposed Q-tap non-linear DF equalizer is also a successive inter-subcarrier interference cancellation scheme. Just like the conventional DF equalizer, it involves the detection of the transmitted symbols on each subcarrier sequentially in a given order. The DF equalization scheme is based on the removal of the interfering signals from the received signal, one at a time as long as they are detected. For example, at the beginning, the subcarrier having the strongest received power can be detected when the interference from other subcarriers is deemed as white noise. Then, the interference caused by the first detected symbol is subtracted from the received signal on the other subcarriers. Therefore, this DF equalizer requires a very complicated computation to determine the optimal detection procedure. Since we are only interested in designing an efficient ICI mitigation algorithm in OFDM, we will not pursue any sophisticated ordering algorithm. In this dissertation, we adopt an arbitrary but fixed order as follows. First we find the subcarrier index with the largest energy by ordering the norms of the columns in the ICI coefficient matrix $\tilde{C}$. Suppose that the received signal on the mth subcarrier has the largest energy. Starting from the mth subcarrier, we detect the subcarrier symbols successively in the forward order, i.e., the detection order is $m, m+1, m+2, \cdots, N-1, 0, 1, \cdots, m-1$. After

determining the subcarrier detection order, we will discuss how each individual subcarrier is detected successively.

As mentioned before, the DF equalizer consists of both feedforward and feedback filters. The objective of the *feedforward matrix* (the collection of the individual subcarrier feedforward equalizer vectors) is to minimize the intercarrier interference from the signals on the undetected subcarriers, which is the residual interference after the subtraction from the previously detected subcarriers. On the other hand, the objective of the feedback filters is to approximate the interference arising from the previously detected subcarriers. It can be verified that a particular choice of the collection of the feedback filters is the original ICI coefficient matrix $\tilde{C}$ such that the interference due to the previously detected subcarriers would be completely canceled if the previous detections are perfect. If the *feedback matrix* (the collection of all feedback equalizer vectors) is set to zero. The DF equalizer becomes a linear equalizer, such as ZF or MMSE linear equalizer. How the Q-tap DF non-linear equalizer works for the OFDM systems will be described in detail as follows.

First, it is assumed that the mth subcarrier has the largest energy. The detected signal for the mth subcarrier $\hat{X}_m$ is obtained using the Q-tap MMSE equalizer based on the received signal vector $\vec{Y}_m^Q$, which is given by Eq. (4.11). The Q-tap MMSE equalizer coefficients are given by Eq. (4.18). The interference induced by the signal on the mth subcarrier, $\vec{U}_m$, is given by

$$\vec{U}_m = \vec{\nu}_m \hat{X}_m, \tag{4.20}$$

where $\vec{\nu}_m$ is the mth column vector of the matrix $\tilde{C}$. Before the other subcarriers are detected, the interference $\vec{U}_m$ is subtracted from the received signal vector $\vec{Y}$ to generate the updated interference-removed signal. The signal on the next subcarrier, the $(m+1)$th subcarrier, $\hat{X}_{m+1}$ is demodulated using the updated interference-removed signal, which is $\vec{Z} = \vec{Y} - \vec{U}_m$. The equalizer for the $(m+1)$th subcarrier is given by Eq. (4.18). However, the equalizer input is based on the updated interference-removed signal, which is updated once a signal on any subcarrier is detected. In general, if we assume $m < k \leq N-1$ and the signals on the subcarriers $m, m-1, \cdots, k-1$ have been detected, the equalizer for the kth subcarrier is determined after the interference from the previously detected signals $\hat{X}_m, \hat{X}_{m+1}, \cdots, \hat{X}_{k-1}$ is subtracted from the received signal. Then, the detected signal on the kth subcarrier is obtained by applying a Q-tap MMSE equalizer on the updated interference-removed signal $\vec{Z}$, which is given by

$$\begin{aligned} \vec{Z} &= \vec{Y} - \sum_{j=m}^{k-1} \vec{U}_m, \quad m < k \leq N-1 \\ &= \vec{Y} - \sum_{j=m}^{k-1} \vec{\nu}_j \hat{X}_j, \end{aligned} \tag{4.21}$$

where $\vec{\nu}_j$ is the jth column vector of the matrix $\tilde{C}$. After detecting the signal on the $N-1$ subcarrier, we will continue with the estimation for the 0th subcarrier, by subtracting the interferences from the signals on the subcarriers $m, m+1, \cdots, N-1$. It means that for $0 \leq k \leq m-1$, the updated interference-removed signal $\vec{Z}$ is given by

$$\vec{Z} = \vec{Y} - \sum_{j=m}^{N-1} \vec{\nu}_j \hat{X}_j - \sum_{j=0}^{k-1} \vec{\nu}_j \hat{X}_j, \quad 0 \leq k \leq m-1. \tag{4.22}$$

From the aforementioned description of the Q-tap DF non-linear equalizer for the OFDM systems, it is found that since the Q-tap MMSE equalization algorithm is used in the DF equalizer, the major computational burden is the inverse of a matrix of size Q-by-Q, just like the Q-tap linear MMSE equalizer. Therefore, the computational complexity of such a DF equalizer is in the same order as that of the Q-tap MMSE equalizer. The performance comparison using the computer simulations between the Q-tap MMSE linear equalizer and the Q-tap DF non-linear equalizer will be addressed in the next sub-section.

4.1.3 Simulation Results for MMSE and DF Equalizers

In this simulation, we test the performances of the Q-tap MMSE equalizer and the DF equalizer discussed in the two previous sub-sections. The parameters are specified as follow. The number of subcarriers is $N = 256$. The COST207 channel model for typical urban areas in [34] is chosen to benchmark the tested OFDM systems. The information symbols are assumed to be modulated as QPSK. Two system performance measures, namely normalized mean-squared error (NMSE) of the equalized output and SER, through Monte Carlo trials are quantified thereby.

First, the Q-tap MSE linear equalizer performances are evaluated. Fig. 4.1 and Fig. 4.2 depict the NMSE performance of the Q-tap MMSE equalizer as a function of SNR when the *maximum OFDM normalized Doppler frequency* ϵ_D is set to be 0.04 and 0.8, while Fig. 4.3 and Fig. 4.4 illustrate the corresponding SER performances. In this simulation, the NMSE of the equalizer is defined as the MSE between the transmitted signal and the equalizer outputs normalized by the transmitted signal energy. The 1-tap, 3-tap, 5-tap, and

the conventional full-tap MMSE equalizers are in contrast. Fig. 4.1 and Fig. 4.3 show that different numbers of taps do not lead to very different performances at a low ϵ_D. In other words, when ϵ_D is small, the ICI power is negligible, and thus the ICI coefficient matrix $\tilde{C}$ is almost diagonal. When ϵ_D is larger, such as $\epsilon_D = 0.8$ in Fig. 4.2 and Fig. 4.4, the performances among different Q-tap equalizers becomes distinguishable, especially when the SNR is high. It is noted that the curve for the conventional full-tap MMSE equalizer approaches to a straight line or the full-tap MMSE equalizer do not lead to an irreducible error probability floor due to the ICI, unlike other Q-tap equalizers. Such an irreducible error probability floor problem becomes obvious for the 1-tap equalizer with $\epsilon_D = 0.8$ in Fig. 4.2 and Fig. 4.4. In addition, the error probability floor decreases as the number of equalizer taps increases. In Fig. 4.2 and Fig. 4.4, the performance margin resulting from the multi-tap equalizers over the 1-tap equalizer is large even in the very low SNR range such as 0dB $\leq$SNR$\leq$ 5dB. This is because the ICI dominates the overall interference-noise level over the background noise.

Fig. 4.5, Fig. 4.6, and Fig. 4.7 show the NMSE performance versus the *maximum OFDM symbol normalized Doppler frequency* ϵ_D when the SNRs are 10dB, 20dB, and 30dB, respectively. Fig. 4.8, Fig. 4.9 and Fig. 4.10 illustrate the SER performance as the function the ϵ_D when the SNRs are 10dB, 20dB and 30dB, respectively. In general, multi-tap MMSE equalizers can lead to the higher performance margin as the SNR increases. When SNR= 20dB and $\epsilon_D = 0.2$, in Fig. 4.6 and Fig. 4.9, the 3-tap MMSE equalizer has a 2dB gain over the 1-tap equalizer but around 2dB loss compared to the full-tap equalizer in

the NMSE sense. Also in the sense of SER, the 3-tap MMSE equalizer achieves a smaller error probability than the 1-tap equalizer but it achieves a higher error rate than the full-tap equalizer, which are shown in Fig. 4.9. When SNR= 30dB, in Fig.4.7 and Fig. 4.10, the 3-tap MMSE equalizer leads to about 4dB gain over the 1-tap equalizer but leads to around 6dB loss compared to the full-tap equalizer in the MSE sense. In the sense of SER, the 3-tap MMSE equalizer achieves a smaller error rate than the 1-tap equalizer but it achieves a higher error rate than the full-tap equalizer, which are shown in Fig. 4.9.

Next, we compare the Q-tap linear MMSE equalizer with the Q-tap nonlinear DF equalizer to suppress the ICI in the sense of SER via computer simulations. When ϵ_D is small in Fig. 4.11, the DF equalizer outperforms the MMSE equalizer with the same number of Q taps at high SNR values. However, when ϵ_D is large in Fig. 4.12 and Fig. 4.13, the DF equalizer outperforms the MMSE equalizer with the same number of Q taps for the entire SNR range of interest. The 5-tap DF equalizer exhibits a considerable performance improvement over the 1-tap DF equalizer in Fig 4.11 and Fig. 4.13. In addition, Fig. 4.13 shows that we can suppress ICI effectively, and improve the SER performance significantly with a very efficient DF equalizer even for the situation that *the maximum OFDM symbol normalized Doppler frequency shift* is up to 0.8.

4.1.4 Summary of ICI Mitigation Equalizers

In Chapter 2, we have investigated the impact of the channel variation natures on the OFDM systems. The channel variations introduce ICI and degrade the OFDM performance. Our analysis revealed that for a given maximum Doppler frequency shift, the major

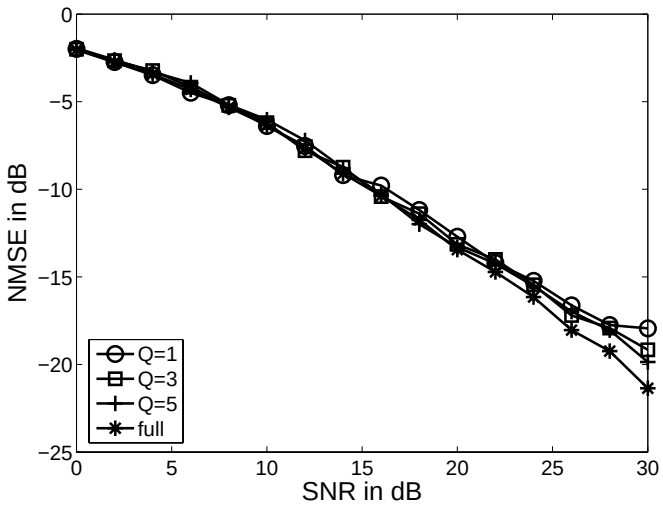

Figure 4.1: NMSE of the Q-tap MMSE Equalizer with $\epsilon_D = 0.04$

ICI power is caused by a few neighboring subcarriers. This fact motivated us to develop the new low-complexity Q-tap equalizers. In this section, two different Q-tap equalizers, namely linear MMSE and non-linear DF equalizers, are designed to suppress the ICI due to the time-varying channel natures in the presence of multiple Doppler frequency shifts. The conventional full-tap MMSE equalizer approach is not feasible, due to the large number of subcarriers in the OFDM systems. Simulation results show that our two Q-tap equalizers both can improve the system performance in the sense of SER with moderate computational complexities. Moreover, the Q-tap nonlinear DF equalizer usually outperforms the Q-tap linear MMSE equalizer at the higher values of *maximum OFDM symbol normalized Doppler frequency.*

For the developments of these equalizers, we assume that the ICI coefficient matrix $\tilde{C}$ is given at the OFDM receiver. However, in reality, the matrix $\tilde{C}$ is usually unknown. Thus, it requires to estimate this unknown matrix prior to the employment of the Q-tap

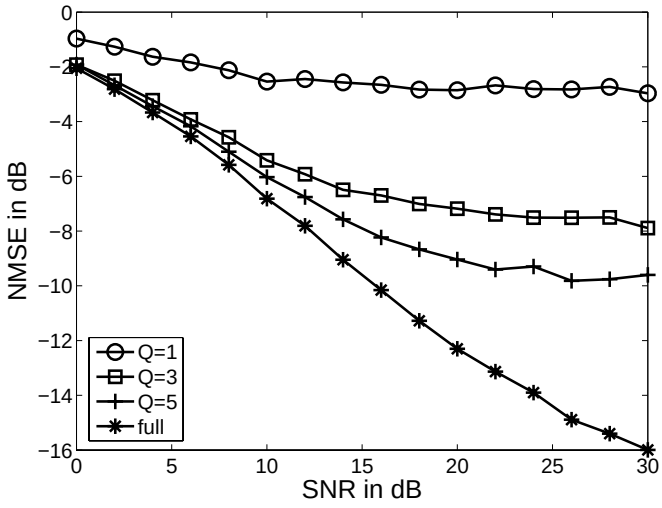

Figure 4.2: NMSE of the Q-tap Equalizer MMSE with $\epsilon_D = 0.8$

equalizers. In the next section, we will address how to estimate this ICI coefficient matrix $\tilde{C}$.

4.2 ICI Coefficient Estimation

The MMSE and DF equalizers in the previous section both require the *channel state information*, or the ICI coefficient matrix $\tilde{C}$ in this dissertation. In contrast to the maximum-likelihood (ML) channel estimation in [37], the Wiener filtering exploits the possibly available information about the statistical properties of the channel and therefore achieves an improved estimation quality. In this section, we investigate a pilot-aided ICI coefficient estimator via this Wiener filtering. The Wiener filter incorporates the channel statistical properties in a WSSUS channel model. We will derive the appropriate Wiener filter for the time-varying WSSUS channel model adopted in the dissertation.

For the channel estimation in a conventional OFDM system, it is often assumed that

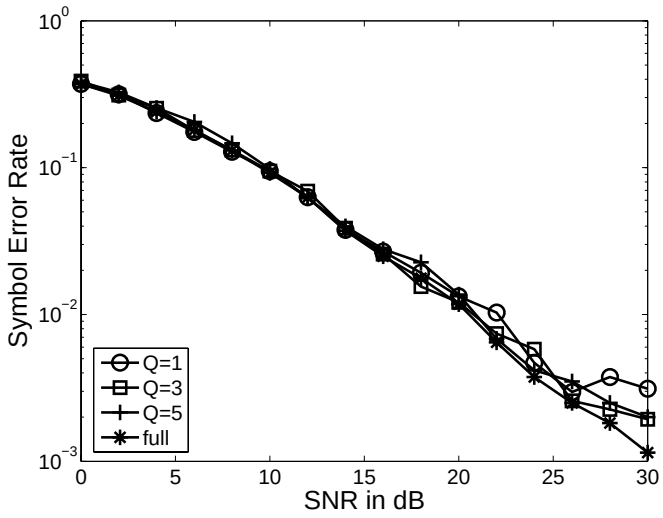

Figure 4.3: Q-tap Equalizer SER with $\epsilon_D = 0.04$

the channel does not change within at least one OFDM symbol period [42]. This assumption is valid for a variety of scenarios, but it is no longer valid for high Doppler frequency shift together with a long OFDM symbol duration. In such a situation, the channel is assumed to be fast time-varying and the ICI coefficient estimator should be restricted to perform on every individual OFDM symbol block. In this section, we propose a pilot-aided ICI coefficient matrix $\tilde{C}$ estimator based on the Wiener filtering for the rapid time-varying channels. Our proposed channel estimation scheme makes use of the channel statistical properties, when the WSSUS channel model is assumed. Unlike other model-free time-varying channel estimators in [25][35] where the pilot symbols are inserted in the time domain, our proposed channel estimation method inserts the pilots before the IFFT in the transmitter in the frequency domain instead. Our strategy will make the proposed channel estimator easily incomparable in the existing OFDM standards. In [25][35], the pilot symbols constitute a Dirac-delta sequence consisting of only one nontrivial data sample

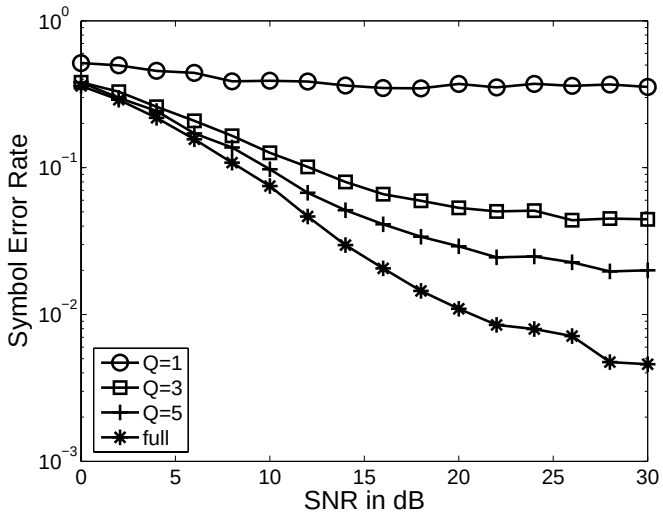

Figure 4.4: Q-tap Equalizer SER with $\epsilon_D = 0.8$

which is surrounded by two balanced subsequences of zero values; the complete channel estimation for one OFDM symbol can be achieved by the linear interpolation based on the assumption that the channel varies in a linear fashion within an OFDM symbol duration. This assumption only holds when the Doppler frequency shift is small [25]. Furthermore, our proposed channel estimator leads to the ICI coefficient matrix $\tilde{C}$ directly, and it is different from the existing channel estimation algorithms in [38][39], where the CIR $h(t, \tau)$ was directly estimated. If the channel varies very fast, much more OFDM pilot symbols are need and it would greatly decrease the system throughput [38]. Moreover, the CIRs between the OFDM pilot symbols were approximated through the linear interpolation based on the same linearity assumption. Our proposed channel estimator directly leads to the ICI coefficient matrix. Thus, the channel is not necessarily required to vary in a linear fashion, and our ICI coefficient estimator relies only on the current received OFDM signal. It could track the channel variations from one OFDM symbol to another.

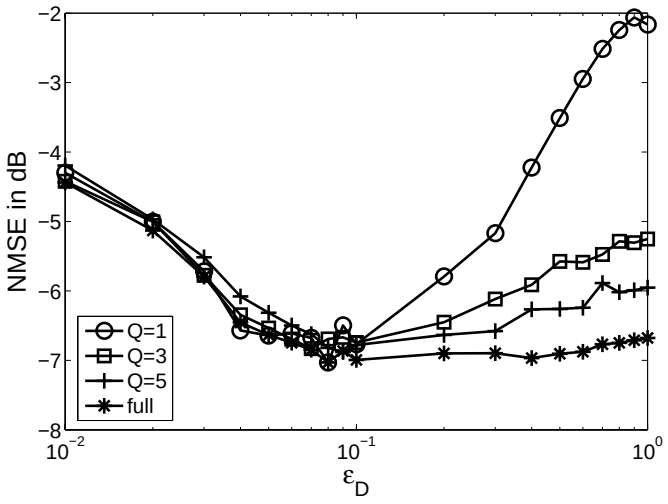

Figure 4.5: NMSE of the Q-tap MMSE Equalizer with SNR = 10dB

This section is organized as follows. First, in Sub-section 4.2.1, we establish the mathematical framework for the Wiener MMSE estimator. Computer simulations are presented in Sub-section 4.2.2. Since the proposed Wiener filter exploits the possibly available channel statistical properties, there may exist a mismatch between the adopted underlying channel model and the actual channel characteristics. The illustration of this channel mismatch problem is also given in Sub-section 4.2.2. Concluding remarks on our proposed pilot-aided ICI coefficient estimator are drawn in Sub-section 4.2.3.

4.2.1 MMSE ICI Coefficient Estimation

We derive the mathematical formula for the ICI coefficient estimator in this subsection. The discrete-time OFDM transmission model in Eq. (2.28) shows that the ICI coefficient matrix $\tilde{C}$ comprises the ICI effect on the transmitted symbol vector $\vec{X}$. Hence, in order to implement the ICI suppression schemes, such as the Q-tap equalizers described in Section 4.1, we have to estimate the ICI coefficients $C_{m,k}$ first. Besides, since the channel

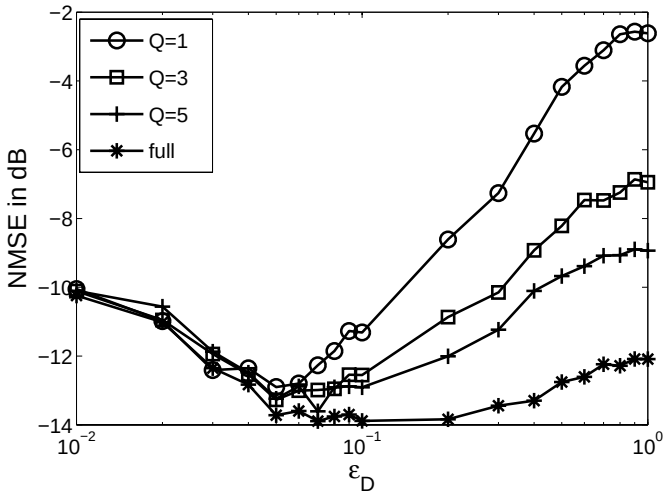

Figure 4.6: NMSE of the Q-tap MMSE Equalizer with SNR = 20dB

is fast time-varying, the estimation of ICI coefficients can depend only on the currently received OFDM symbol block. For this purpose, we design a linear MMSE estimator, as known as the Wiener filter, for each element $C_{m,k}$ of $\tilde{C}$. The estimation of $C_{m,k}$ is achieved using a linear combination of the currently received signal $\vec{Y}$ such that

$$\hat{C}_{m,k} = \vec{v}_{m,k}^{H}\vec{Y}, \quad 0 \leq m,k \leq N-1, \tag{4.23}$$

where $\hat{C}_{m,k}$ denotes the estimate of $C_{m,k}$, the Winer filter coefficient $\vec{v}_{m,k}$ is obtained by minimizing the MSE between $\hat{C}_{m,k}$ and $C_{m,k}$, i.e.,

$$\vec{v}_{m,k} = \underset{\vec{v}_{m,k}}{argmin}\, E\left\{|C_{m,k} - \vec{v}_{m,k}^{H}\vec{Y}|^2\right\}. \tag{4.24}$$

According to [67], the solution to Eq. (4.24) can be stated as follows. First, $E\left\{|C_{m,k} - \vec{v}_{m,k}^{H}\vec{Y}|^2\right\}$ is calculated as

$$\begin{aligned} & E\left\{|C_{m,k} - \vec{v}_{m,k}^{H}\vec{Y}|^2\right\} \qquad (4.25)\\ = \;& E\left\{\left(C_{m,k} - \vec{v}_{m,k}^{H}\vec{Y}\right)\left(C_{m,k}^{*} - \vec{Y}^{H}\vec{v}_{m,k}\right)\right\} \end{aligned}$$

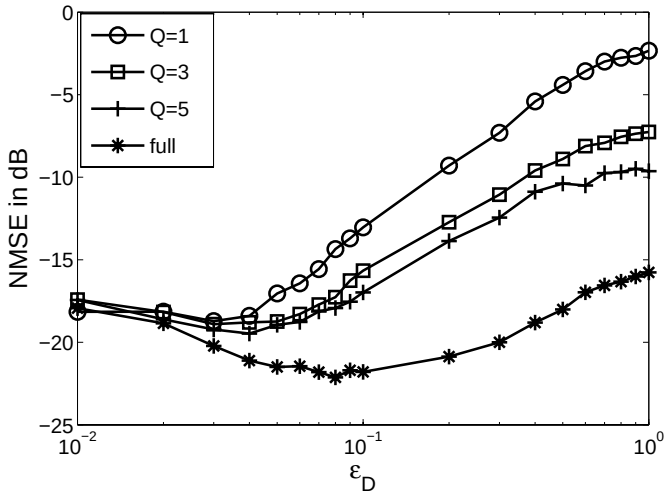

Figure 4.7: NMSE of the Q-tap MMSE Equalizer with SNR = 30dB

$$= E\left\{C_{m,k}C_{m,k}^*\right\} - E\left\{C_{m,k}\vec{Y}^H\right\}\vec{v}_{m,k} - \vec{v}_{m,k}^H E\left\{\vec{Y}C_{m,k}^*\right\} + \vec{v}_{m,k}^H E\left\{\vec{Y}\vec{Y}^H\right\}\vec{v}_{m,k}.$$

Secondly, differentiating Eq. (4.25) with respect to $\vec{v}_{m,k}$ and setting it to zero, we have the solution to Eq. (4.24) as follows

$$\vec{v}_{m,k} = \tilde{R}_{\vec{Y}\vec{Y}^H}^{-1}\vec{\rho}_{C_{m,k}\vec{Y}}, \tag{4.26}$$

where $\tilde{R}_{\vec{Y}\vec{Y}^H}$ is the auto-correlation matrix of the received signal $\vec{Y}$, which is defined in Eq. (4.2), and $\vec{\rho}_{C_{m,k}\vec{Y}}$ is the cross-correlation between the received signal $\vec{Y}$ and $C_{m,k}$, i.e.,

$$\vec{\rho}_{C_{m,k}\vec{Y}} \equiv E\left\{C_{m,k}\vec{Y}\right\}. \tag{4.27}$$

For the optimum Wiener filter coefficients given by Eq. (4.26), the corresponding MSE of the estimation is also obtained as [67]:

$$MSE = \sigma_{m,k}^2 - \vec{\rho}_{\vec{Y}C_{m,k}}^H \tilde{R}_{\vec{Y}\vec{Y}^H}^{-1}\vec{\rho}_{\vec{Y}C_{m,k}}, \tag{4.28}$$

where $\sigma_{m,k}^2 \equiv E\left\{C_{m,k}C_{m,k}^*\right\}$, which is given by Eq. (2.40). In the following, we will determine $\tilde{R}_{\vec{Y}\vec{Y}^H}$ and $\vec{\rho}_{C_{m,k}\vec{Y}}$ based on the transmission model given by Eq. (2.28), using the

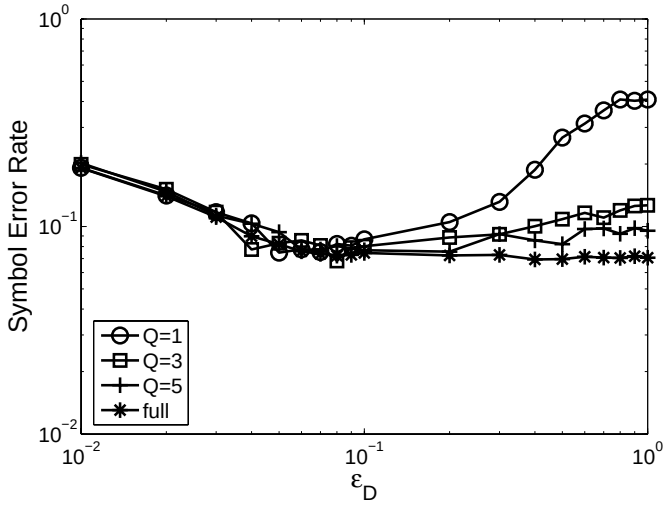

Figure 4.8: Q-tap MMSE Equalizer SER with SNR=10dB

statistical properties of the time-varying WSSUS channel described in section 2.2.

A. Calculation of $\tilde{R}_{\vec{Y}\vec{Y}^H}$

According to Eq. (4.2), $\tilde{R}_{\vec{Y}\vec{Y}^H}$ is the auto-correlation matrix of the received signal $\vec{Y}$. Let β_{m_1,m_2} with $0 \leq m_1, m_2 \leq N-1$ denote an element in the auto-correlation matrix $\tilde{R}_{\vec{Y}\vec{Y}^H}$. According to the definition of $\tilde{R}_{\vec{Y}\vec{Y}^H}$, β_{m_1,m_2} is written as $\beta_{m_1,m_2} \equiv E\left\{Y_{m_1}Y_{m_2}^*\right\}$. Using the assumption that $\vec{X}$ and $\vec{W}$ are uncorrelated, we can derive β_{m_1,m_2} as follows:

$$\begin{aligned}
\beta_{m_1,m_2} &= E\left\{\left(\sum_{k_1=0}^{N-1} X_{k_1}C_{m_1,k_1}\right)\left(\sum_{k_2=0}^{N-1} X_{k_2}C_{m_2,k_2}\right)^*\right\} + E\left\{W_{m_1}W_{m_2}^*\right\} \quad (4.29)\\
&= E\left\{\sum_{k_1=0}^{N-1}\sum_{k_2=0}^{N-1} X_{k_1}X_{k_2}^*C_{m_1,k_1}C_{m_2,k_2}^*\right\} + E\left\{W_{m_1}W_{m_2}^*\right\}\\
&= \sum_{k_1=0}^{N-1}\sum_{k_2=0}^{N-1} E\left\{X_{k_1}X_{k_2}^*\right\}E\left\{C_{m_1,k_1}C_{m_2,k_2}^*\right\} + E\left\{W_{m_1}W_{m_2}^*\right\}.
\end{aligned}$$

The autocorrelation of the transmitted signal X_k, $E\left\{X_{k_1}X_{k_2}^*\right\}$, is calculated as follow. Define the set $\mathcal{S}_{\mathrm{p}}$, which consists of N_p subcarrier indexes on which the pilot

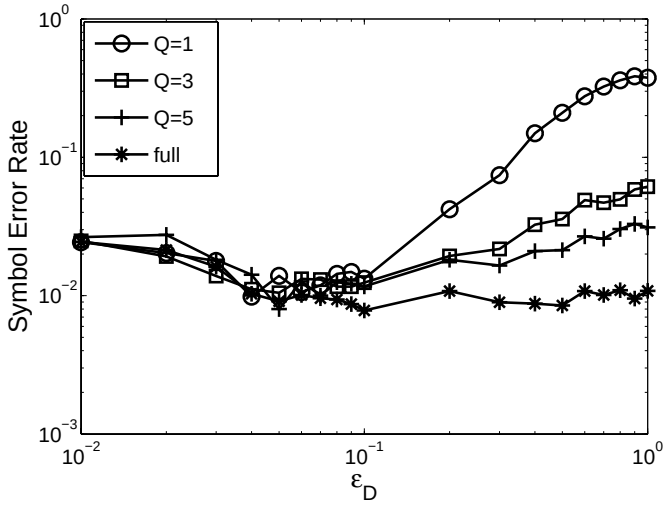

Figure 4.9: Q-tap MMSE Equalizer SER with SNR=20dB

symbols are transmitted. Thus, X_k is a pilot signal if $k \in \mathcal{S}_{\mathrm{p}}$. Therefore,

$$E\left\{X_{k_1}X_{k_2}^*\right\} = \begin{cases} X_{k_1}X_{k_2}^*, & if \quad k_1, k_2 \in \mathcal{S}_{\mathrm{p}} \\ E_s\delta\left(k_1 - k_2\right), & if \quad k_1, k_2 \notin \mathcal{S}_{\mathrm{p}} \\ 0, & otherwise \end{cases} . \tag{4.30}$$

Next we proceed with the calculation of the cross-correlation between ICI coefficients C_{m_1,k_1} and C_{m_2,k_2}. From Eq. (2.26), we obtain

$$\begin{aligned} & E\left\{C_{m_1,k_1}C_{m_2,k_2}^*\right\} \qquad (4.31) \\ = \; & \frac{1}{N^2}\sum_{l=0}^{L-1}\sum_{l'=0}^{L-1}\sum_{n=0}^{N-1}\sum_{n'=0}^{N-1} E\left\{e^{\frac{-j2\pi(k_1+\epsilon_l)l}{N}}e^{\frac{j2\pi\left(k_2+\epsilon_{l'}\right)l'}{N}}\gamma_{l,n}\gamma_{l',n'}^* e^{\frac{-j2\pi(m_1-k_1-\epsilon_l)n}{N}}e^{\frac{j2\pi\left(m_2-k_2-\epsilon_l'\right)n'}{N}}\right\}. \end{aligned}$$

Now, the WSSUS properties of the time-varying channel described by Eqs. (2.12), (2.13), (2.15) and (2.35) can be applied to simplify Eq. (4.31), such that

$$\begin{aligned} & E\left\{C_{m_1,k_1}C_{m_2,k_2}^*\right\} \qquad (4.32) \\ = \; & \frac{1}{N^2}\sum_{n=0}^{N-1}\sum_{n'=0}^{N-1}\sum_{l=0}^{L-1} e^{\frac{-j2\pi(k_1-k_2)l}{N}}\phi_h\left(n-n'\right)\phi_\tau(\tau_l)e^{\frac{-j2\pi(m_1-k_1)n+j2\pi(m_2-k_2)n'}{N}}E\left\{e^{\frac{j2\pi(n-n')\epsilon_l}{N}}\right\} \end{aligned}$$

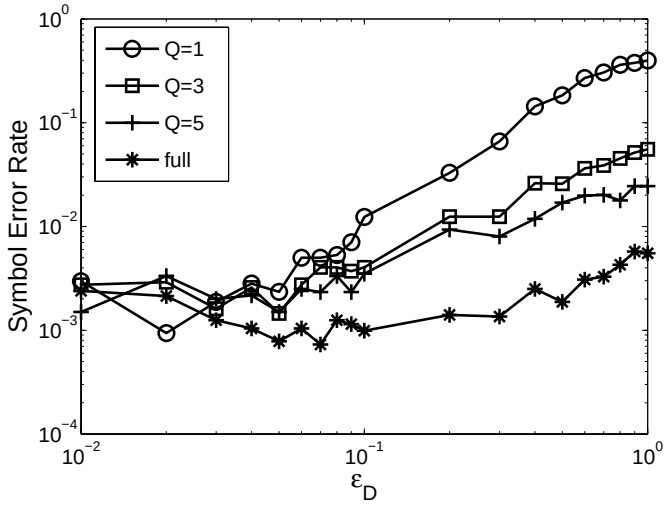

Figure 4.10: Q-tap MMSE Equalizer SER with SNR=30dB

$$= \frac{1}{N^2}\sum_{n=0}^{N-1}\sum_{n'=0}^{N-1}\phi_h\left(n-n'\right)e^{\frac{-j2\pi(m_1-k_1)n+j2\pi(m_2-k_2)n'}{N}}J_0\left(\frac{2\pi\left(n_1-n_2\right)\epsilon_D}{N}\right)\sum_{l=0}^{L-1}e^{\frac{-j2\pi(k_1-k_2)l}{N}}\phi_\tau(\tau_l).$$

Let us defined $\Upsilon(k_1-k_2)\equiv\sum_{l=0}^{L-1}e^{\frac{-j2\pi(k_1-k_2)l}{N}}\phi_\tau\left(\tau_l\right)$, where $\phi_\tau\left(\tau_l\right)$ is the multipath intensity profile of the channel, which is defined in Eq. (2.13). Several multipath intensity profiles for different wireless channel models are given in [34]. If $k_1=k_2$, $\Upsilon(k_1-k_2)$ is simplified to be 1. And if $k_1\neq k_2$, $\Upsilon(k_1-k_2)$ depends on the adopted channel model. It is noted that no close-form expression for Eq. (4.32) can be available while the numerical evaluation has to take place. The last term in Eq. (4.29) is the auto-correlation of the noise, W_k, which is given by Eq. (2.25c). Summarizing all of the derived results, we obtain the ultimate expression for β_{m_1,m_2}, which is given by

$$\begin{aligned}&\beta_{m_1,m_2} \qquad (4.33)\\ &= \frac{\sigma_s^2}{N^2}\sum_{k\notin\mathcal{S}_{\mathrm{p}}}\sum_{n=0}^{N-1}\sum_{n'=0}^{N-1}\phi_h\left(n-n'\right)e^{\frac{-j2\pi(m_1-k)n+j2\pi(m_2-k)n'}{N}}J_0\left(\frac{2\pi\left(n_1-n_2\right)\epsilon_D}{N}\right)\\ &+ \frac{1}{N^2}\sum_{\substack{k_1=0\\k_1\in\mathcal{S}_{\mathrm{p}}}}^{N-1}\sum_{\substack{k_2=0\\k_2\in\mathcal{S}_{\mathrm{p}}}}^{N-1}X_{k_1}X_{k_2}^{*}\Upsilon(k_1-k_2)\end{aligned}$$

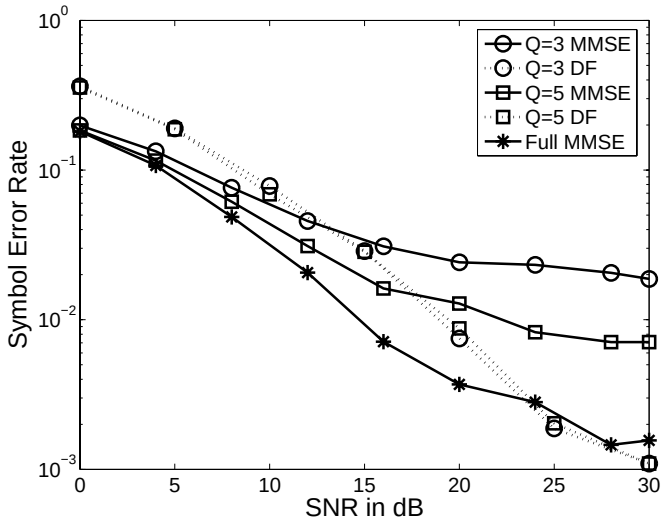

Figure 4.11: SER of the Q-tap MMSE and DF Equalizers with $\epsilon_D = 0.08$

$$\sum_{n=0}^{N-1}\sum_{n'=0}^{N-1}\phi_h\left(n-n'\right)e^{\frac{-j2\pi(m_1-k_1)n+j2\pi(m_2-k_2)n'}{N}}J_0\left(\frac{2\pi\left(n_1-n_2\right)\epsilon_D}{N}\right)$$
$$+\quad \sigma_W^2\delta(m_1-m_2).$$

Since $\tilde{R}_{\vec{Y}\vec{Y}^H}$ is constant for estimating every $\hat{C}_{m,k}$, we do not need to re-calculate $\tilde{R}_{\vec{Y}\vec{Y}^H}$ for estimating a new element $C_{m,k}$ in $\tilde{C}$ each time.

B. Calculation of $\vec{\rho}_{\vec{Y}C_{m,k}}$

According to Eq. (4.27), $\vec{\rho}_{\vec{Y}C_{m,k}}$ is the cross-correlation between the received signal $\vec{Y}$ and the ICI coefficient $C_{m,k}$. Let ρ_{m_1}, for $0 \le m_1 \le N-1$, represent an element in the cross-correlation vector $\vec{\rho}_{\vec{Y}C_{m,k}}$. According to Eq. (4.27), ρ_{m_1} can be calculated as

$$\begin{aligned}\rho_{m_1} &= E\left\{Y_{m_1}C_{m,k}^*,\right\} \qquad (4.34)\\ &= E\left\{\left(\sum_{k_1=0}^{N-1}X_{k_1}C_{m_1,k_1}+W_{m_1}\right)C_{m,k}^*\right\}\\ &= E\left\{\sum_{k_1=0}^{N-1}X_{k_1}C_{m_1,k_1}C_{m,k}^*\right\}+E\left\{W_{m_1}C_{m,k}^*\right\}.\end{aligned}$$

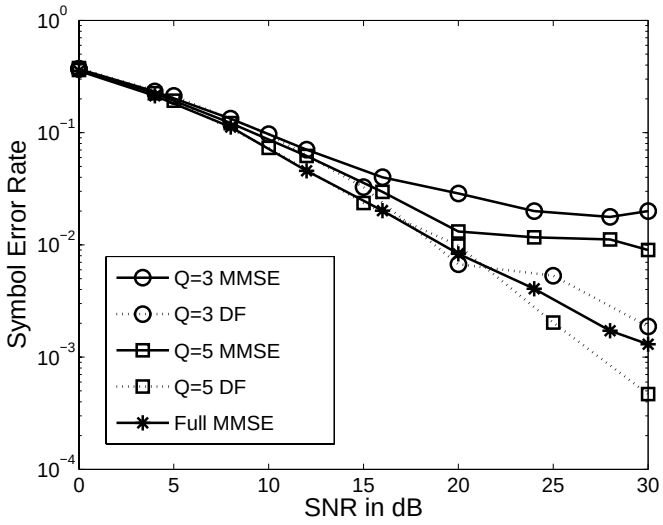

Figure 4.12: SER of the Q-tap MMSE and DF Equalizers with $\epsilon_D = 0.4$

It is assumed that the ICI coefficient $C_{m,k}$ and AWGN W_k are uncorrelated, the second term in Eq. (4.34) becomes zero. Therefore, Eq. (4.34) yields

$$\rho_{m_1} = \sum_{k_1=0}^{N-1} E\{X_{k_1}\} E\left\{C_{m_1,k_1} C_{m,k}^*\right\}. \tag{4.35}$$

If the transmitted signal X_{k_1} is not a pilot signal, we obtain

$$E\{X_{k_1}\} = 0. \tag{4.36}$$

In summary, the cross-correlation between the received signal $\vec{Y}$ and the ICI coefficient $C_{m,k}$ is given by

$$\rho_{m_1} = \sum_{\substack{k_1=0 \\ k_1 \in \mathcal{S}_\mathrm{p}}}^{N-1} X_{k_1} E\left\{C_{m_1,k_1} C_{m,k}^*\right\}, \tag{4.37}$$

where $E\left\{C_{m_1,k_1} C_{m,k}^*\right\}$ is given in Eq. (4.32) by setting $m_2 = m$ and $k_2 = k$. Substituting Eqs. (4.33) and (4.37) into Eq. (4.24), we can determine the optimum Wiener filter coefficients $\vec{v}_{m,k}$ for estimating the ICI coefficient $C_{m,k}$ according to Eq. (4.24). Once the ICI coefficient matrix $\tilde{C}$ is obtained, the equalizer schemes proposed in

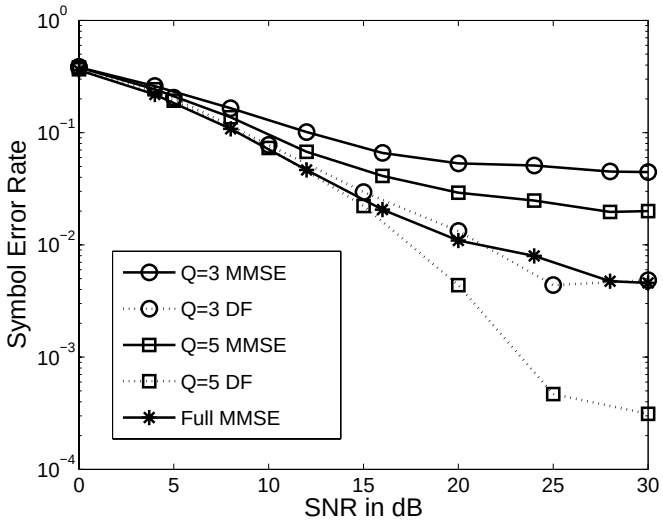

Figure 4.13: SER of the Q-tap MMSE and DF Equalizers with $\epsilon_D = 0.8$

Section 4.1 can be deployed to mitigate the ICI, and thus improve the overall system performance.

Since the calculation of the cross-correlation vector $\vec{\rho}_{\vec{Y}C_{m,k}}$ depends on the subcarrier indexes m and k, the optimum MMSE ICI coefficient estimator $\vec{v}_{m,k}$ given by Eq. (4.26) will in general be different for each element in the ICI coefficient matrix $\tilde{C}$. It means that a huge computational burden is required for estimating $\tilde{C}$ especially for a large number of subcarriers. However, as we mentioned in the Section 4.1, a Q-tap equalizer would reduce the computational complexity by only sacrificing a slight performance degradation. Therefore, instead of trying to estimate every element in the matrix $\tilde{C}$, we only need to estimate a certain elements in the $\tilde{C}$ matrix, which are the elements given in Eq. (4.13c). In this way, we do not have to estimate the complete $\tilde{C}$.

Practically, the proposed pilot-aided Wiener filter for estimating the ICI coefficient matrix $\tilde{C}$ is computationally heavy especially for a large number of subcarriers. However, the auto-correlation matrix $\tilde{R}_{\vec{Y}\vec{Y}^H}$ of the received signal given by Eq. (4.33) and the cross-correlation vector $\vec{\rho}_{m,k}$ in Eq. (4.37) can be calculated in advance at the receiver if we know the channel statistics beforehand. It is reasonable to assume that the channel statistical properties do not dramatically change very often. Therefore, it is not necessary the calculate $\tilde{R}_{\vec{Y}\vec{Y}^H}$ and $\vec{\rho}\rho_{m,k}$ frequently once a new incoming signal is available at the receiver. This would greatly reduce the computational complexity. However, another problem arises from this employment. There exists a mismatch between the actual channel characteristics and the pre-established channel statistics where a particular estimator is designed. It is obvious that the performance of the pilot-aided Wiener filter based ICI coefficient estimator will degrade. To obtain the insights into the performance of the ICI coefficient estimators, Monte Carlo simulation results are presented in the next sub-section. Also, this channel mismatch problem is investigate through the simulations in the next sub-section.

4.2.2 ICI Coefficient Estimation Simulation Results

To evaluate the performance of our derived optimum MMSE ICI coefficient matrix $\tilde{C}$ estimator, we present the Monte Carlo simulation results here. The underlying parameters are the same as those in Sub-section 4.1.3.

The MSE performance of the ICI coefficient estimation is defined as

$$MSE \equiv \frac{1}{N^2} \sum_{m=0}^{N-1} \sum_{k=0}^{N-1} |\hat{C}_{m,k} - C_{m,k}|^2. \tag{4.38}$$

We depict the MSE curves versus the SNR in Fig. 4.14 and Fig. 4.15 where the *maximum OFDM symbol normalized Doppler frequency* ϵ_D is set as 0.08 and 0.4, respectively. In these simulations, different pilot overheads in one OFDM symbol block are considered. The overhead ratios between the number of pilots and the total number of subcarriers, i.e., $\frac{N_p}{N}$, are illustrated for different curves in the figures. According to Figures 4.14 and 4.15, the MSE curves appear to have error floors. It is noted that the error floor level decreases as the number of pilot symbols in one OFDM symbol increases, and the error floor level increases as the *maximum OFDM symbol normalized Doppler frequency shift* increases.

Since the proposed pilot-aided ICI coefficient estimation algorithm requires the

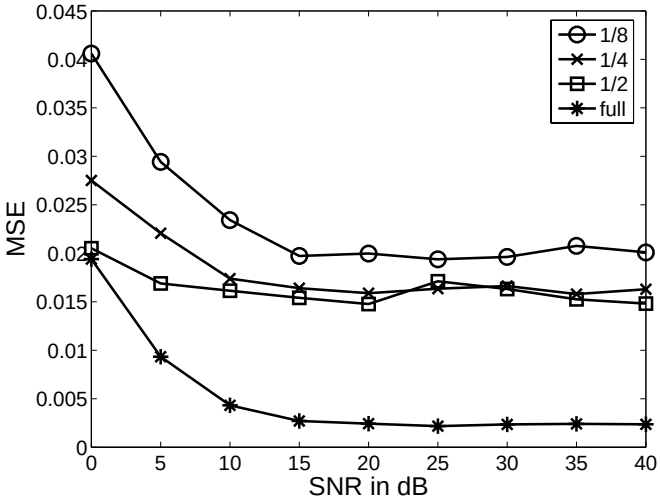

Figure 4.14: MSE of $\tilde{C}$ estimation with $\epsilon_D = 0.08$

knowledge of the channel's statistical properties, and in practice, the actual channel characteristics is almost always unknown, there may exist a mismatch in between. Hence our proposed ICI coefficient estimation algorithm performance would degrade. To study this mismatch problem, we provide Figures 4.16, 4.17 and 4.18 to illustrate this phenomenon.

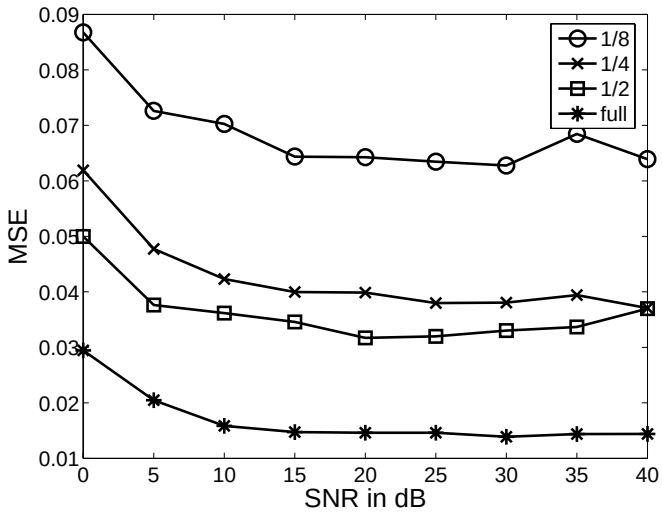

Figure 4.15: MSE of $\tilde{C}$ estimation with $\epsilon_D = 0.4$

In Figure 4.16, the *maximum OFDM symbol normalized Doppler frequency* is mismatched. The actual *maximum OFDM symbol normalized Doppler frequency* is set as 0.1 but the *maximum OFDM symbol normalized Doppler frequency* for the pilot-aided ICI coefficient estimation is set as 0.6. It is observed from Figure 4.16 that the mismatch in *maximum OFDM symbol normalized Doppler frequency* obviously increases the MSE. However, the MSE performance margin caused by this mismatch is less than that due to the decrease in the number of pilot symbols. For the extreme case which is labeled as "full" in the figures, if all transmitted symbols are pilots, the MSE performance margin due to the *maximum OFDM symbol normalized Doppler frequency* mismatch is negligible.

In the next simulation, we assume that the *maximum OFDM symbol normalized Doppler frequency* is perfectly known, and there exists a mismatch between the actual channel multipath intensity profile $\phi_\tau(\tau_l)$ and the pre-set multipath intensity profile. Figures 4.17 and 4.18 depict the MSE curves versus SNR when the *maximum OFDM symbol*

normalized Doppler frequency are set as 0.1 and 0.3, respectively. According to Figures 4.17 and 4.18, we observe that the MSE performance margin due to this multipath intensity profile mismatch are negligible for all kinds of pilot overheads and different *maximum OFDM symbol normalized Doppler frequencies*. According to Figures 4.16, 4.17 and 4.18, we can conclude that the mismatch in the Doppler frequencies dominates the MSE performance margin over the mismatch in the channel multipath intensity profiles since the mobility is the crucial factor in the wireless communications.

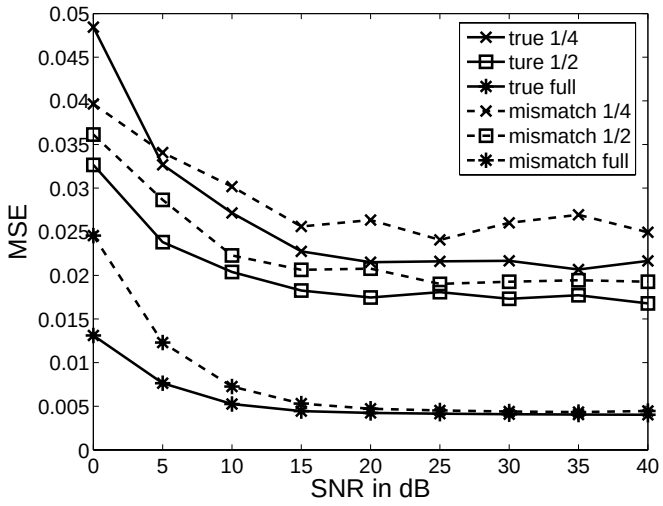

Figure 4.16: MSE of $\tilde{C}$ estimation with ϵ_D mismatch

4.2.3 Summary for ICI Coefficient Estimation

We have derived a pilot-aided ICI coefficient estimator for the OFDM in the rapid time-varying environments, which is based on the MMSE Wiener filtering. Our proposed algorithm utilizes the correlation properties of the channels. From the simulation results, we can conclude that the time-varying nature of the channel, rather than the channel mismatch, is the dominant effect in this pilot-aided Wiener filtering based ICI coefficient

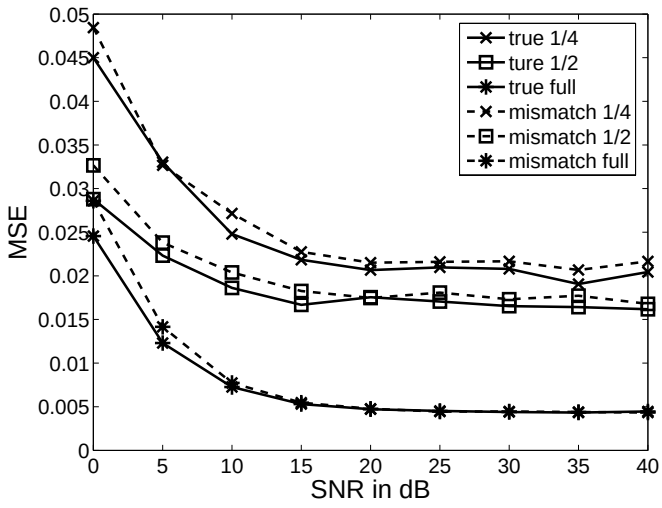

Figure 4.17: MSE of $\tilde{C}$ estimation with $\phi_\tau(\tau_l)$ mismatch

estimation scheme. Furthermore, if only a single OFDM symbol is available at the receiver, our proposed scheme will suffer from an irreducible error floor when the ICI dominates all kinds of interferences and noise due to the time-varying nature of the channels. And it is also observed that as the number of pilots increases, the system throughput and the error floor decrease. It means that the proposed ICI coefficient estimator could achieve a better MSE performance in the sacrifice of the system throughput. Finally, from the simulation results, we can conclude that the Doppler frequency mismatch dominates in the performance degradation.

Once the ICI coefficient matrix $\tilde{C}$ is estimated, the linear MMSE or the non-linear DF equalizers could be employed at the receiver to mitigate the ICI, and thus improve the system performance. In the next section, the simulation results, which are obtained from the OFDM system incorporating the pilot-aided Wiener filtering based ICI coefficient estimations with the Q-tap equalizers in Section 4.1, are presented to test the overall

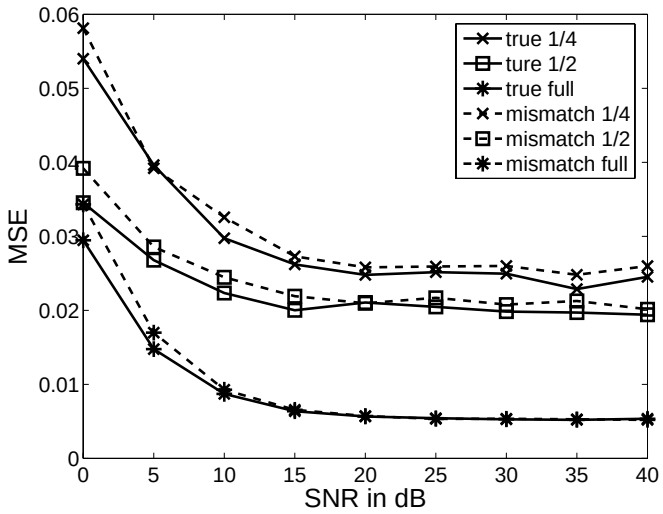

Figure 4.18: MSE of $\tilde{C}$ estimation with $\phi_\tau(\tau_l)$ mismatch

performance improvements over the fast time-varying fading channels.

4.3 ICI Mitigation Summary

Based on the analysis in Chapter 2, we propose the Q-tap linear MMSE and non-linear DF equalizers in the frequency domain to suppress the ICI in Section 4.1. It was demonstrated that due to the large number of subcarriers in one OFDM symbol N, the conventional MMSE equalizer which involves an N-by-N matrix inverse as shown in Eq. (4.2) is not feasible. In addition, based on the ICI property investigated in Section 2.3.2, the computation complexity of the conventional MMSE equalizer could be significantly reduced using the Q-tap equalizers in Section 4.1 in a slight trade-off of the SER performance. In Section 4.2, a pilot-aided ICI coefficient estimator via the Wiener filtering was designed under the WSSUS channel model assumption. To conclude this chapter, we incorporate the Q-tap equalizers with the ICI coefficient estimator to test the overall system performance in terms of the SER. The system parameters comply with those in Sub-section 4.1.3. The

pilot overhead is $\frac{1}{16}$ per OFDM symbol block. The *maximum OFDM symbol normalized Doppler frequencies* are set as 0.06 and 0.8. SNR varies from 0dB to 30dB. The performances of a 7-tap linear MMSE and a 7-tap non-linear DF equalizers are tested. The modulation schemes are QPSK and 16QAM. The following are the simulation results.

Figure 4.19 depicts the symbol error rate as the function of SNR when the *maximum OFDM symbol normalized Doppler frequency* ϵ_D is set as 0.06. If we compare the SER curves in Figures 2.9 and 4.19, we observe that our proposed ICI mitigation scheme, in which a Q-tap equalizer incorporated with the MMSE ICI coefficient estimation algorithm, greatly outperforms the conventional OFDM system with a one-tap equalizer. It is also observed that for the 16QAM modulation, two aforementioned equalizers lead to almost the same performance. For the QPSK modulation, the DF non-linear equalizer outperforms the MMSE linear equalizer. As the SNR increases, the performance margin using the DF non-linear equalizer over the MMSE linear equalizer becomes large.

Figure 4.20 illustrates the SER as the function of SNR when the *maximum OFDM symbol normalized Doppler frequency* ϵ_D is set as 0.8. According to Figure 4.20, we discover that at high *maximum OFDM symbol normalized Doppler frequency* values in Figure 4.20, our proposed ICI mitigation technique still outperforms the conventional OFDM receiver with a one-tap equalizer.

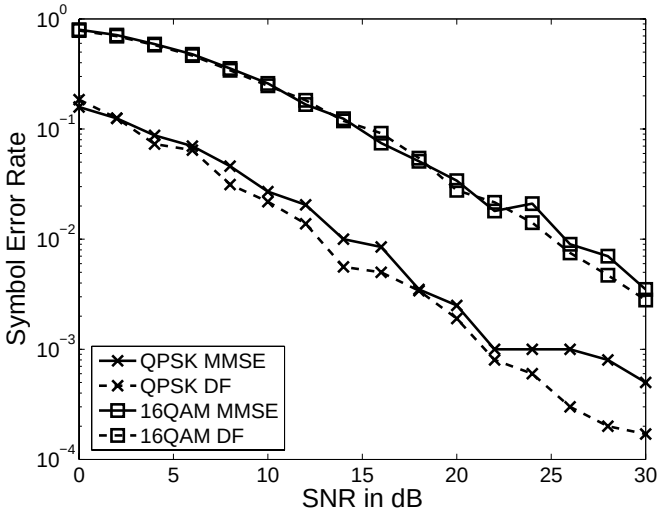

Figure 4.19: SER after ICI mitigation with $\epsilon_D = 0.06$

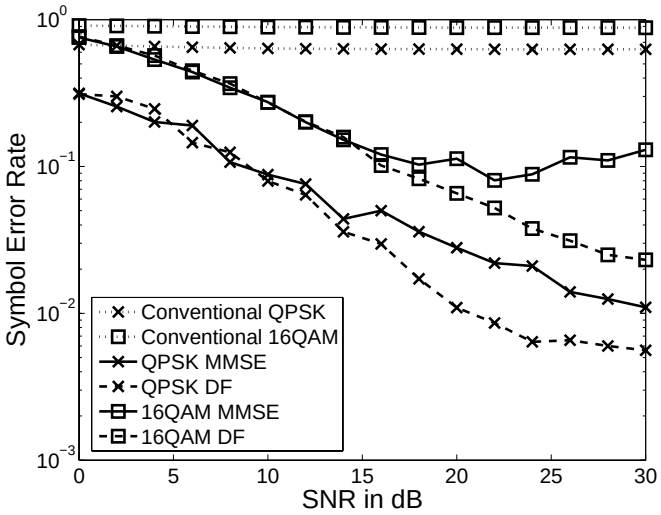

Figure 4.20: SER after ICI mitigation with $\epsilon_D = 0.8$

Chapter 5

An Alternative ICI Mitigation Algorithm

In this chapter, an alternative proposed algorithm using the second approach as stated in the previous section 3.2 is introduced and it is based on the ICI self-cancellation precoder [19][20]. In the ICI self-cancellation precoder scheme, the redundancies are made by repeating the information symbols twice or more prior to the OFDM modulation for the future ICI cancellation at the receiver. Specifically we fix the ICI self-cancellation precoder with a coding rate 1/2 for now and $\tilde{B}$ in the precoder matrix $\tilde{\Theta}$ of Eq. (3.2) becomes

$$\tilde{B} = \sqrt{\frac{1}{2}} \begin{bmatrix} 1 \\ \\ -1 \end{bmatrix}. \tag{5.1}$$

At the receiver, the ICI self-cancellation decoder is simply implemented as a differential decoder [19][20], such that the decoded signal before symbol detection can be obtained as

$$\begin{aligned} e_k &= Y_{2k} - Y_{2k+1} \quad 0 \le k \le N/2 - 1 \\ &= (\alpha_k - \alpha_{2k+1}) d_m + I_{2k} - I_{2k+1} + W_{2k} - W_{2k+1} \\ &= \varsigma_k d_k + n_k, \end{aligned} \tag{5.2}$$

where $\varsigma_k = \alpha_k - \alpha_{2k+1}$, I_{2k} and I_{2k+1} are the ICIs for the subcarrier Y_{2k} and Y_{2k+1}, respectively, which are defined in Eq. (2.26). The aggregate noise $n_k = I_{2k} - I_{2k+1} + W_{2k} - W_{2k+1}$ can be well approximated as an additive Gaussian process as long as N is large by the central limit theorem.

Typically, the decoded signal in Eq. (5.2) should be directly sent for the maximum *a posteriori* (MAP) probability detection to obtain the symbol estimates [19][20]. However, the crucial ambiguity problems arise for the time-varying channel in the presence of multiple Doppler frequencies [69]. Since ς_k is unknown, the phase and amplitude ambiguities caused by ς_k as defined in Eq. (5.2) would severely limit the symbol detection accuracy. Therefore, we propose a novel phase and amplitude estimation algorithm here to solve this ambiguity problem associated with ς_k using an expectation-maximization (EM) [68]-based scheme [69].

The previously described ambiguities can be characterized as the following terminologies: *composite phase*, defined as $\zeta_k \equiv \angle(\varsigma_k)$ and *composite amplitude*, defined as $\varrho_k \equiv |\varsigma_k|$ for the kth subcarrier. Consequently, Eq. (5.2) can be reformulated as

$$e_k = \varrho_k e^{j\zeta_k} d_k + n_k, \quad 0 \le k \le \frac{N}{2} - 1. \tag{5.3}$$

The time-varying characteristics of ς_k induces the changes of these composite phases and composite amplitudes. The statistical estimation technique, EM algorithm, is therefore applied here to track the time-varying parameters ζ_k and ϱ_k. For a QPSK or QAM constellation, the ICI self-cancellation decoded signal in Eq. (5.2) is complex-valued. Since the probability density function of the random process e_k can obviously be described by a complex Gaussian mixture model [68] according to Eq. (5.3), we can transform complex-valued e_k into two-dimensional vectors for convenience. Thus, the real and imaginary parts of e_k can be expressed in a vector form as

$$\vec{E}_k \equiv [\Re(e_k) \quad \Im(e_k)]^T. \tag{5.4}$$

The signal vectors $\vec{E}_k$ in Eq. (5.4) form a two-dimensional Gaussian mixture process [68] with cluster mean vectors related to the signal constellation. The signal constellation vectors in M-QAM can be denoted as $\vec{S}_m = [S_r, S_i]^T, m = 1, 2, \cdots, M$. According to Eq. (5.3) and Eq. (5.4), the associated conditional probability density function can be written as

$$p_{\vec{E}_k|\left\{\vec{o}_m, \tilde{\Delta}_m\right\}_{m=1,2,\cdots,M}} = \sum_{m=1}^{M} \frac{P_m e^{-\frac{1}{2}\left(\vec{E}_k - \vec{o}_m\right)^T \tilde{\Delta_m}^{-1}\left(\vec{E}_k - \vec{o}_m\right)}}{\sqrt{(2\pi)^2 \left|\tilde{\Delta}_m\right|}}, \tag{5.5}$$

where $\vec{o}_m$ is the cluster mean, $\tilde{\Delta}_m$ is the covariance matrix and P_m is the *a priori* probability of the constellation symbol $\vec{S}_m$, for $m = 1, 2, \cdots, M$. Following Eq. (5.3), the cluster mean $\vec{o}_m$ for the constellation symbol $\vec{S}_m$ can be obtained as

$$\begin{aligned} \vec{o}_m &= E\left\{\varrho_k e^{j\zeta_k} \vec{S}_m\right\}, \quad 1 \le m \le M \\ &= \varrho_k \begin{bmatrix} \cos(\zeta_k) & -\sin(\zeta_k) \\ \sin(\zeta_k) & \cos(\zeta_k) \end{bmatrix} \vec{S}_m. \end{aligned} \tag{5.6}$$

Hence, the *average composite phase* can be approximated as

$$\begin{aligned} \hat{\zeta} &= \frac{2}{N} \sum_{k=0}^{\frac{N}{2}-1} \zeta_k \\ &\approx \frac{1}{M} \sum_{m=1}^{M} \arctan\left(\frac{o_{i,m}}{o_{r,m}} - \frac{S_{i,m}}{S_{r,m}}\right). \end{aligned} \tag{5.7}$$

The *average composite amplitude* can be approximated as

$$\begin{aligned} \hat{\varrho} &= \sqrt{\frac{2}{N} \sum_{k=0}^{\frac{N}{2}-1} \varrho_k^2} \\ &\approx \frac{\sqrt{\sum_{m=1}^{M} \| \vec{o}_l \|^2}}{\sqrt{\sum_{m=1}^{M} \| \vec{S}_l \|^2}}. \end{aligned} \tag{5.8}$$

According to Eq. (5.7) and Eq. (5.8), it is clear that the estimated average composite phase $\hat{\zeta}$ and the estimated average composite amplitude $\hat{\varrho}$ can be determined once the cluster mean vectors $\vec{M}_l$ are estimated. The following is our proposed algorithm to estimate the cluster mean vectors $\vec{o}_m$ and solve the problem of phase and amplitude ambiguities.

The cluster mean vectors $\vec{o}_m$ and the covariance matrices $\tilde{\Delta}_m$ in Eq. (5.5) are considered as the parameters to be estimated. Given the Gaussian mixture probability density function in Eq. (5.5), expectation-maximization (EM) based estimation algorithm can be applied to determine the optimal maximum-likelihood estimates for $\vec{o}_m$ and $\tilde{\Delta}_m$ [68]. The estimates can be obtained through the maximum-likelihood estimation procedure such that

$$\left\{\hat{\vec{o}}_m, \hat{\tilde{\Delta}}_m\right\}_{m=1,2,\cdots,M} \tag{5.9}$$

$$= argmax\left\{\log\left(p_{\vec{E}_k|\left\{\vec{o}_m,\tilde{\Delta}_m\right\}_{m=1,2,\cdots,M}}\right)\right\}, \tag{5.10}$$

where $p_{\vec{E}_k|\left\{\vec{o}_m,\tilde{\Delta}_m\right\}_{m=1,2,\cdots,M}}$ is given by Eq. (5.5).

To search for the optimal estimates of the cluster mean vectors and the covariance matrices in Eq. (5.9), the iterative EM algorithm in [68] can be applied. The simulation results and the details of this algorithm can be found in [69].

Chapter 6

Conclusion

We conclude this dissertation here. This dissertation provides a solution to improve the OFDM system performance using the ICI mitigation techniques for the fast time-varying fading channels in the presence of multiple Doppler frequency shifts. The time-varying fading channels with multiple Doppler frequency shifts would destroy the orthogonality among subcarriers in OFDM, and result in the ICI, which leads to an irreducible error probability floor. This error probability floor is proportional to the *maximum OFDM symbol normalized Doppler frequency shift*. Accordingly, we propose a time-varying ICI coefficient estimator incorporated with new Q-tap equalizers to suppress the ICI for a better detection performance.

In this dissertation, first, We study the impact of the channel variations in the presence of multiple Doppler frequency shifts on the OFDM performance. We also analyze the ICI power due to the time-varying natures of the mobile channels. We discover that the ICI power arises from just a few adjacent subcarriers. We also show that as *the maximum OFDM symbol normalized Doppler frequency shift* increases, more neighboring subcarriers are involved to interfere the subject subcarrier. These studies motivate us to the design the low-complexity Q-tap equalizers (MMSE linear equalizer and DF non-linear equalizer) for the ICI suppression. The MMSE linear equalizer exhibits the error probability floor when *the maximum OFDM symbol normalized Doppler frequency shift* is large, while the

DF non-linear equalizer can achieve the better SER performance. Both equalizers can outperform the conventional OFDM system with a one-tap equalizer.

To employ these equalizers at the receiver to suppress the ICI, the channel state information is also required. The time-varying channel estimation and tracking are very challenging, especially when the channel experiences multipath fadings. In this dissertation, we design a pilot-aided linear ICI coefficient estimator based on the Winer filtering. Our proposed channel estimator utilizes the channel statistical properties. Furthermore, we have investigated the performance margins due to the *the maximum OFDM symbol normalized Doppler frequency shift* and the multipath intensity profile mismatches. According to our experiments, the number of pilot signals in one OFDM symbol rather than the channel statistical mismatch is the dominant factor of the OFDM performance. Therefore, our proposed pilot-aided ICI coefficient estimation algorithm using the Wiener filtering is shown to be robust over the time-varying channel characteristics.

On the other hand, we have also introduced an alternative ICI mitigation algorithm which depends on the ICI self-cancellation coding. The associated phase and amplitude ambiguity problems are discussed. The EM-based approach to solve the ambiguity problems is also presented in this dissertation.

There still remain several issues for the future research. For example, if two or more OFDM symbols are acquired, the error probability floor of our proposed pilot-aided ICI coefficient estimation algorithm using the Wiener filtering would vanish. In this situation,

more sophisticated channel statistical properties are required to re-calculate the ICI coefficient matrix $\tilde{C}$. Moreover, instead of the ICI coefficient matrix $\tilde{C}$ estimates are carried out, which are independent from one OFDM symbol to another, we could develop a new estimation algorithm to adaptively track the changes in the ICI coefficients. Future study on how to explore the correlations between the ICI coefficient matrices for different OFDM symbol blocks can be pursued.

References

[1] A. F. Molisch, L. B. Lopes, M. Paier, J. Fuhl, and E. Bonek, "Error floor of unequalized wireless personal communications systems with MSK modulation and training-sequence-based adaptive sampling," *IEEE Trans. Commun.,* vol. 45, no. 5, pp. 554-562, May 1997.

[2] M. Paier, A. F. Molisch, and E. Bonek, "Training-sequence-based determination of optimum sampling time in unequalized TDMA mobile radio systems," *IEEE Trans. on Vehicular Technology,* vol. 49, no. 4, pp. 1408-1415, July 2000.

[3] A. F. Molisch and J. Fuhl, "Bit error probability of differentially detected (G)MSK in unequalized mobile radio channels," *IEEE 46th Vehicular Technology Conference, 1996, 'Mobile Technology for the Human Race',* vol 2, 28 April-1 May 1996, pp. 1404-1408.

[4] J. G. Proakis, *Digital Communications*, Fourth Edition, McGraw-HILL Science/Engineering/Math International Edition, 2001.

[5] M. Mouly and M.-B. Pautet, *The Gsm System for Mobile Communications*, Telecom Pub., 1992.

[6] P. A. Bello, "Selective Fading Limitations of the Kathryn Modem and Some System Design Considerations," *IEEE Trans. Commun.,* vol. 13, no. 3, pp. 320-333, Sept. 1965.

[7] L. J. Cimini, "Analysis and Simulation of a Digital Mobile Channel Using Orthogonal Frequency Division Multiplexing," *IEEE Trans. Commun.,* vol. 33, no. 7, pp. 665-675, July 1985.

[8] European Telecommunications Standards Institute, *Radio Broadcasting systems: Digital Audio Broadcasting (DAB) to Mobile, Portable, and Fixed Receivers,* 2nd. Sophia Antipolis, France, May 1997. ETS300 401.

[9] European Broadcasting Union, *Digital Video broadcasting Framing Structure, Channel Coding, and Modulation for Digital Terrestrial Television* Geneva, Switzerland, Jan. 1999. Draft EN300 744 V1.2.1.

[10] *Part 11: Wireless LAN Medium Access Control (MAC) and Physical layer (PHY)*

Specifications: High-Speed Physical layer in the 5 GHz Band, IEEE Standard 802.11-1999.

[11] *Local and Metropolitan Area Networks-Part 16, Air Interface for Fixed Broadband Wireless Access Systems,* IEEE Standard 802.16a.

[12] *Draft IEEE Standard for Local and metropolitan area networks, Part 16: Air Interface for Fixed and Mobile Broadband Wireless Access Systems Amendment for Physical and Medium Access Control Layers for Combined Fixed and Mobile Operation in Licensed Bands*, IEEE P802.16e/D8, May, 2005.

[13] T. Keller and L. Hanzo, "Adaptive multicarrier modulation: a convenient framework for time-frequency processing in wireless communications," *Proceedings of the IEEE,* vol. 88, no. 5, pp. 611-640, May 2000.

[14] S. Weinstein and P. Ebert, "Data Transmission by Frequency-Division Multiplexing Using the Discrete Fourier Transform," *IEEE Trans. Commun.,* vol. 19, no. 5, pp. 628-634, 1971.

[15] M. Speth, S. A. Fechtel, G. Fock, and H. Meyr, "Optimum receiver design for wireless broad-band systems using OFDM. I," *IEEE Trans. Commun.,* vol. 47, no. 11, pp. 1668-1677, Nov. 1999.

[16] S. G. Kang, Y. M. Ha and E. K. Joo, "A comparative investigation on channel estimation algorithms for OFDM in mobile communications," *IEEE Trans. on Broadcasting,* vol. 49, no. 2, pp. 142-149, June 2003.

[17] M. Morelli, and U. Mengali, "A comparison of pilot-aided channel estimation methods for OFDM systems," *IEEE Trans. Signal Processing,* vol. 49, no. 12, pp. 3065-3073, Dec. 2001.

[18] M. Russell and G. L. Stuber, "Interchannel interference analysis of OFDM in a mobile environment," *1995 IEEE 45th Vehicular Technology Conference*, vol. 2, 25-28 July 1995, pp. 820-824.

[19] Y. Zhao and S.-G. Haggman, "Sensitivity to Doppler shift and carrier frequency errors in OFDM systems-the consequences and solutions," *IEEE 46th Vehicular Technology Conference, 1996, 'Mobile Technology for the Human Race',* vol. 3, 28 April-1 May 1996, pp. 1564-1568.

[20] Y. Zhao and S.-G. Haggman, "IIntercarrier interference self-cancellation scheme for OFDM mobile communication systems," *IEEE Trans. Commun.,* vol. 49, no. 7, pp. 1185-1191, July 2001.

[21] P. Robertson and S. Kaiser, "Analysis of the loss of orthogonality through Doppler spread in OFDM systems," *GLOBECOM '99, Global Telecommunications Conference, 1999.* vol. 1B, Dec. 1999, pp. 701-706.

[22] J. Li and L. J. Cimini, "Bounds on the interchannel interference of OFDM in time-varying impairments," *IEEE Trans. Commun.,* vol.49, no.3, pp. 401-404, Mar. 2001.

[23] J. Li and M. Kavehrad, "Effects of time selective multipath fading on OFDM systems for broadband mobile applications," *IEEE Commun. Letters,* vol.3, no.12, pp. 332-334, Dec. 1999.

[24] P. Chen and H. Kobayashi, "Maximum likelihood channel estimation and signal detection for OFDM systems," *IEEE ICC 2002,* vol. 3, 28 April-2 May 2002, pp. 1640-1645.

[25] W. G. Jeon, K. H. Chang and Y. S. Cho, "An equalization technique for orthogonal frequency-division multiplexing systems in time-variant multipath channels," *IEEE Trans. Commun.,* vol. 47, no. 1, pp. 27-32, Jan. 1999.

[26] P. A. Bello, "Characterization of Randomly Time-Variant Linear Channels," *IEEE Trans. Commun.,* vol. 11, no. 4, pp.360-393, Dec. 1963.

[27] J. S. Sadowsky and V. Kafedziski, "On the correlation and scattering functions of the WSSUS channel for mobile communications," *IEEE Trans. Vehicular Technology,* vol. 47, no. 1, pp. 270-282, Feb. 1998.

[28] W. C. Jakes, *microwave Mobile Communications*, The Institute of Electrical and Electronics Engineers, Inc. New York, A John Wiley & Sons, Inc., 1974.

[29] P. H. Moose, "A technique for orthogonal frequency division multiplexing frequency offset correction," *IEEE Trans. Commun.,* vol. 42, no. 10, pp. 2908-2914, Oct. 1994.

[30] P. Robertson and S. Kaiser, "The effects of Doppler spreads in OFDM(A) mobile radio systems," *VTC 1999-Fall, IEEE VTS 50th Vehicular Technology Conference, 1999,* vol. 1, 19-22 Sept. 1999, pp. 329-333.

[31] I. S. Gradshteyn and I. M. Ryzhik, *Tables of series, Products, and Integrals,* 5th ed., vol. I and II, Frankfurt: Harri Deutsch, 1981.

[32] T. Ojanpera, J. Castro, D. Emmer, M. Gudmundson, P. Jung, A. Klein, G. Kramer, R. Pirhonen, L. Rademacher, J. Skold and A. Toskala, "FRAMES-hybrid multiple access technology," *IEEE 4th International Symposium on Spread Spectrum Techniques and Applications Proceedings, 1996,* vol. 1, 22-25 Sept. 1996, pp. 320-324.

[33] C. Tellambura, Y. J. Guo, S. K. Barton, "Equaliser Performance for HIPERLAN in indoor channels," *Wireless Personal communications,* vol. 3, no. 4, pp. 397-410, 1996.

[34] A. F. Molisch, *Wideband wireless digital communications*, Prentice Hall, 2001.

[35] E. Leung and P. Ho, "A successive interference cancellation scheme for an ODFM system," *ICC 98, 1998 IEEE International Conference on Communications,* vol. 1, 7-11 June 1998, pp.375-379.

[36] M. Munster and L. Hanzo, "Second-order channel parameter estimation assisted cancellation of channel variation-induced inter-subcarrier interference in OFDM systems," *International Conference on EUROCON'21, trends in Communications,* vol. 1, 4-7 July 2001, pp. 1-5.

[37] C. Kuo and J.-F. Chang, "Equalization and channel estimation for OFDM systems in time-varying multipath channels," *PIMRC 2004. 15th IEEE International Symposium on Personal, Indoor and Mobile Radio Communications,* vol. 1, 5-8 Sept. 2004, pp. 474-478.

[38] Y.-S. Choi, P. J. Voltz, and F. A. Cassara, "On channel estimation and detection for multicarrier signals in fast and selective Rayleigh fading channels," *IEEE Trans. Commun.,* vol. 49, no. 8, pp. 1375-1387, Aug. 2001.

[39] O. Simeone, Y. Bar-Ness and U. Spagnolini, "Pilot-based channel estimation for OFDM systems by tracking the delay-subspace," *IEEE Trans. Wireless Commun.,* vol. 3, no. 1, pp. 315-325, Jan. 2004.

[40] W. T. Ng and V. K. Dubey, "On coded pilot based channel estimation for OFDM in very fast multipath fading channel," *Proceedings of the 2003 joints conference of the Fourth International conference on Information, Communications and signal processing and the Fourth Pacific Rim conference on multimedia,* vol. 2, 15-18 Dec. 2003, pp. 850-863.

[41] Y. Li, L. J. Cimini and N. R. Sollenberger, "Robust channel estimation for OFDM systems with rapid dispersive fading channels," *IEEE Trans. Commun.,* vol. 46, no. 7, pp. 902-915, July 1998.

[42] F. Tufvesson and T. Maseng, "Pilot assisted channel estimation for OFDM in mobile cellular systems," *IEEE 47th Vehicular Technology Conference,* vol. 3, 4-7 May 1997, pp. 1639-1643.

[43] S. Chen and T. Yao, "Intercarrier interference suppression and channel estimation for OFDM systems in time-varying frequency-selective fading channels," *IEEE Trans. Consumer Electronics,* vol. 50, no. 2. pp. 429-435, May 2004.

[44] S. Tomasin, A. Gorokhov, Y. Haibing and J.-P. Linnartz, "Iterative interference cancellation and channel estimation for mobile OFDM," *IEEE Trans. Wireless Commun.,* vol. 4, no. 1, pp. 238-245, Jan. 2005.

[45] A. Gorokhov and J.-P. Linnartz, "Robust OFDM receivers for dispersive time-varying channels: equalization and channel acquisition," *IEEE Trans. Commun.,* vol. 52, no. 4, pp. 572-583, Apr. 2004.

[46] K.-Y. Han, S.-W. Lee, J.-S. Lim and K.-M. Sung, "Channel estimation for OFDM with fast fading channels by modified Kalman filter," *IEEE Trans. Consumer Electronics,* vol. 50, no. 2, pp.443-449, May 2004.

[47] Y.-H. Yeh and S.-G. Chen, "Reduction of Doppler-induced ICI by interference prediction," *PIMRC 2004, 15th IEEE International Symposium on Personal, Indoor and Mobile Radio Communications,* vol. 1, 5-8 Sept. 2004, pp. 653-657.

[48] X. Qian and L. Zhang, "Interchannel interference cancellation in wireless OFDM systems via Gauss-Seidel method," *ICCT 2003, International Conference on Communication Technology Proceedings,* vol. 2, 9-11 April 2003, pp. 1051-1055.

[49] G. Li, H. Yang, L. Cai and L. Gui, "A low-complexity equalization technique for OFDM system in time-variant multipath channels," *VTC 2003-Fall, IEEE 58th Vehicular Technology Conference,* vol. 4, 6-9 Oct. 2003, pp. 2466-2470.

[50] S. Chen, G. Dai and T. Yen, "Zero-forcing equalization for OFDM systems over doubly-selective fading channels using frequency domain redundancy," *IEEE Trans. Consumer Electronics,* vol. 50, no. 4, pp. 1004-1008. Nov. 2004.

[51] P. Schniter, "Low-complexity equalization of OFDM in doubly selective channels," *IEEE Trans. Signal Processing,* vol. 52, no. 4, pp. 1002-1011, April 2004.

[52] X. Cai and G. B. Giannakis, "Bounding performance and suppressing intercarrier interference in wireless mobile OFDM," *IEEE Trans. Commun.,* vol. 51, no. 12, pp.2047-2056, Dec. 2003.

[53] J. Armstrong, "Analysis of new and existing methods of reducing intercarrier interference due to carrier frequency offset in OFDM," *IEEE Trans. Commun.,* vol. 47, no. 3, pp. 365-369, Mar. 1999.

[54] J. Y. Yun and Y. H. Lee, "A bandwidth efficient precode to reduce intercarrier interference in OFDM," *VTC 2004-Spring, IEEE 59th Vehicular Technology Conference,* vol. 2, 17-19 May 2004 , pp. 944-946.

[55] L. Yang, C. Ming, S. Cheng, H. Wang, "Intercarrier interference cancellation in OFDM mobile systems," *2004 IEEE Eighth International Symposium on Spread Spectrum Techniques and Applications,* 30 Aug.-2 Sept. 2004, pp. 449-453.

[56] H. Yang, G. Li, L. Cai and L. Gui, "Performance of turbo product codes in OFDM systems with ICI self-cancellation over fast fading channel," *VTC 2004-Spring, IEEE 59th Vehicular Technology Conference,* vol. 2, 17-19 May 2004, pp. 1019-1022.

[57] A. Seyedi and G. J. Saulnier, "General ICI self-cancellation scheme for OFDM systems," *IEEE Trans. Vehicular Technology,* vol. 54, no. 1, pp. 198-210, Jan. 2005.

[58] H. Zhang and Y. Li, "Optimum frequency-domain partial response encoding in OFDM system," *IEEE Trans. Commun.,* vol. 51, no. 7, pp. 1064-1068, July 2003.

[59] Y. Zhao; J.-D. Leclercq and S.-G. Haggman, "Intercarrier interference compression in OFDM communication systems by using correlative coding," *IEEE Commun. Letters,* vol. 2, no. 8, pp. 214-216, Aug. 1998.

[60] Y. Qiao, S. Yu, P. Su and L Zhang, "Research on an iterative algorithm of LS channel estimation in MIMO OFDM systems," *IEEE Trans. Broadcasting,* vol. 51, no. 1, pp 149-153, March 2005.

[61] A. Stamoulis, S. N. Diggavi and N. Al-Dhahir, "Intercarrier interference in MIMO OFDM," *IEEE Trans. Signal Processing,* vol. 50, no. 10, pp 2451-2464, Oct. 2002.

[62] L. L. Scharf, *Statistical signal processing: detection, estimation and time series analysis,* Reading, Mass. : Addison-Wesley Pub. Co., 1991.

[63] G. J. Foschini Jr. And M. J. Gans, "On limits of wireless communication in a fading environment when using multiple antennae," *Wireless Personal Commun.,* vol. 6, no. 3, pp. 311-335, Mar. 1998.

[64] D. Agrawal, V. Tarokh, A. Naguib and N. Seshadri, "Space-time coded OFDM for high data-rate wireless communication over wideband channels," *VTC 98, 48th IEEE Vehicular Technology Conference,* vol. 3, 18-21 May 1998, pp. 2232-2236.

[65] S. U. H. Qureshi, "Adaptive equalization," *Proceedings of the IEEE,* vol. 73, no. 9, pp. 13491387, Sept. 1985.

[66] M. K. Varanasi, "Decision feedback multiuser detection: a systematic approach," *IEEE Trans. Information Theory,* vol. 45, no. 1, pp. 219-240, Jan. 1999.

[67] S. Haykin, *Adaptive filter theory,* 4th edition, Prentice-Hall, 2002.

[68] A. P. Dempster, N. M. Laird, and D. B. Rubin, "Maximum likelihood from incomplete data via the EM algorithm," *Journal of the Royal Statistical Society,* ser. B, vol. 39, no. 1, pp. 1-38, 1977.

[69] H. C. Wu and X. Huang, "Joint Phase/Amplitude estimation and symbol detection for wireless ICI self-cancellation coded OFDM systems," *IEEE Trans. on Broadcasting,* vol. 50, no. 1, pp. 49-55, March 2004.

Vita

Xiaozhou Huang was born in Xi'an City, ShaanXi Province, People's Republic of China. She received the bachelor's and master's degrees in wireless communication from the Northern Jiaotong University, Beijing, China, in 1993 and 1996, respectively, and the master's degree in physics science from the Physical Department and the master's degree in digital signal processing from the Electrical and Computer Engineering Department from the University of Massachusetts, Dartmouth, Massachusetts, in 1999 and 2002 respectively. She worked for Beijing University of Post and Telecommunication-NORTEL research lab from 1996 to 1998. She entered the graduate program in the Department of Electrical and Computer Engineering at Louisiana State University in Fall 2003. She is currently working toward the degree of Doctor of Philosophy in electrical engineering. Her research interests are in the areas of digital communication and communication theory.